VALIDATION OF ERS-1 ENVIRONMENTAL DATA PRODUCTS

A Final Report

Submitted to:
National Aeronautics and Space Administration
Earth Science and Applications Division
Washington, DC 20546

Prepared by:
Mark A. Goodberlet and Calvin T. Swift
Microwave Remote Sensing Laboratory
University of Massachusetts
Amherst, MA 01003

John C. Wilkerson
Satellite Research Laboratory, NOAA/NESDIS
Washington, D.C. 20746

Effective date: March 1, 1992
Preparation date: November 10, 1994

Executive Summary

Evaluation of the launch–version algorithms used by the European Space Agency (ESA) to derive wind field and ocean wave estimates from measurements of sensors aboard the European Remote Sensing satellite, ERS–1, has been accomplished through comparison of the derived parameters with coincident measurements made by 24 open ocean buoys maintained by the National Oceanic and Atmospheric Administration (NOAA). During the period from November 1, 1991 through February 28, 1992, data bases with 577 and 485 pairs of coincident sensor/buoy wind and wave measurements were collected for the Active Microwave Instrument (AMI) and Radar Altimeter (RA) respectively. Based on these data, algorithm retrieval accuracy is estimated to be ± 4 m/s for AMI wind speed, ± 3 m/s for RA wind speed and ± 0.6 m for RA wave height. After removing $180°$ ambiguity errors, the AMI wind direction retrieval accuracy was estimated at $\pm 28°$. All of the ERS–1 wind and wave retrievals are relatively unbiased. These results should be viewed as interim since improved algorithms are under development. As final versions are implemented, additional assessments should be conducted to complete the validation.

Chapter 1
Pre-Launch Validation Activities for ERS-1

1.0 Introduction

Pre-launch validation activities consisted of 1) the modification and testing of existing processing software used in the validation of SSM/I and GEOSAT, and the testing of this modified software with simulated ERS-1 data, 2) determination of the error structure of the validation process for the AMI and RA winds (due to lack of information on algorithms for the RA significant wave height and the ATSR sea surface temperature, no error structure calculations for these parameters have been made for this report). 3) estimation of the required number of satellite/buoy observations needed for validation, and 4) calculation of the total data sets to be expected from the NOAA buoy network for each retrieved parameter, for both the 3-day and 35-day repeat cycles. This work was carried out at the University of Massachusetts, Amherst, MA, in the Microwave Remote Sensing Laboratory (MIRSL) at the University of Massachusetts.

1.1 Validation Software

The necessary data for completing the modifications to the validation processing software were provided by ESRIN. This included a computer compatible tape (CCT) containing simulated ERS-1 data with software to read the tape, code for the boundary layer model used to adjust wind speed measurements taken at different elevations above the sea surface, and ERS-1 swath and orbit visualization software. These data packages were integrated into the existing processing software and tested end-to-end using the simulated ERS-1 data. In addition, modifications were made to accommodate the continuous wind measurements from the buoys. This change permits a more accurate match of the time series averages of the buoy winds with the spatial averages of winds from the AMI and RA.

1.2 Error Structure

The errors due to uncertainties in the measurements of the winds from the buoys and satellite were calculated using instrument noise figures and retrieval algorithms provided by ESRIN and the NOAA Data Buoy Center. The following error estimates were derived using AMI noise figure from *Carter [1990]*, AMI CMOD1 algorithm from *Long [1987]*, RA noise figure from "Applications and scientific uses of ERS-1 radar altimeter data" an ESA report, RA wind speed algorithm from Dobson [1987], and buoy measurement accuracy figures from *Gilhousen [1986]*. The noise figures used for comparison of buoy-measured winds with remotely-sensed winds are from *Pierson [1983]*.

Figure 1 presents the wind speed dependence of the comparison error for AMI and buoy wind speeds for an AMI beam incidence angle of 40°. Curves a_1 and a_2 represent the speed-dependent errors associated with the matching of time-averaged continuous 10-minute and 8.5 minute buoy winds with the instantaneous spatially-averaged winds from the AMI. The difference in comparison errors between the two is due to the improved match of the ground truth when using the continuous 10-minute averages of wind speed
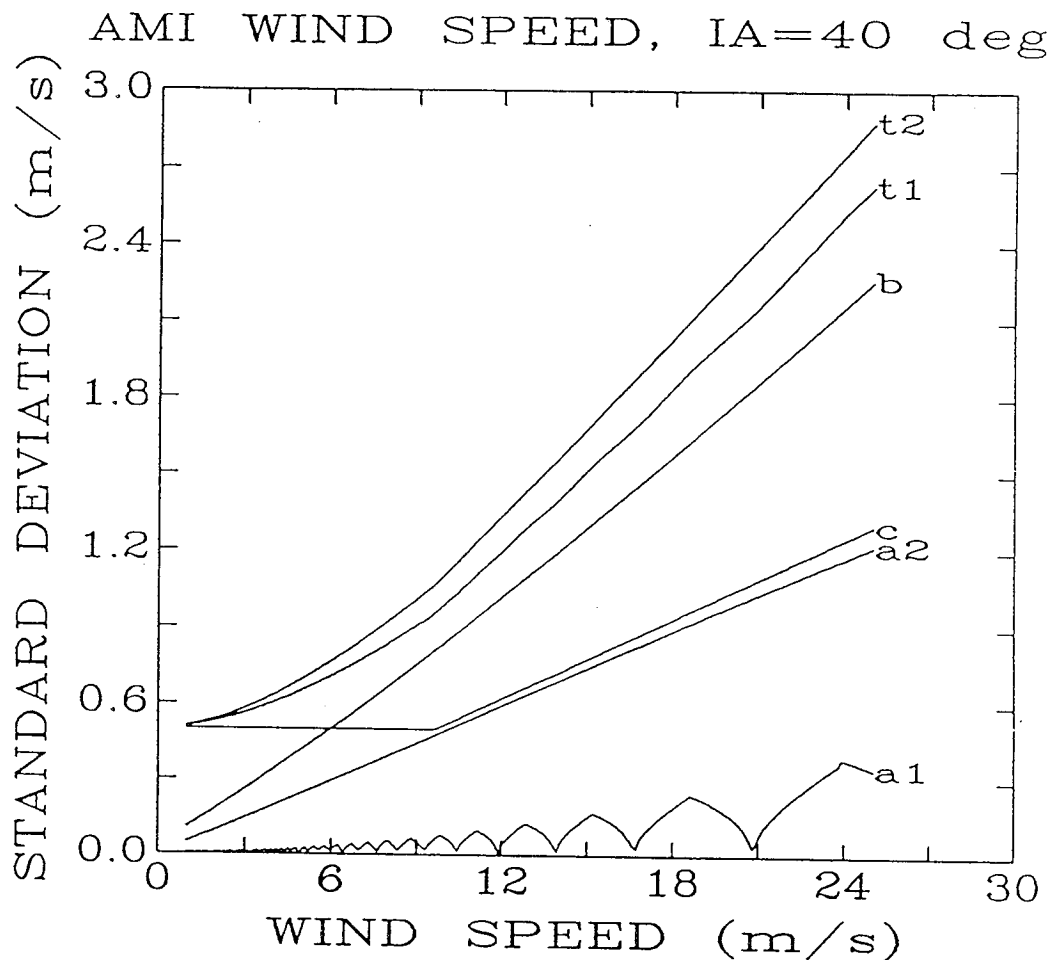
Figure 1. Wind speed dependence of the comparison error for AMI and buoy wind speeds for an AMI beam incidence angle of 40°. Curves a_1 and a_2 represent the speed-dependent errors associated with the matching of time-averaged continuous 10-minute and 8.5 minute buoy winds with the instantaneous spatially-averaged winds from the AMI. Curve b represent errors due to AMI noise, and curve c to errors related to buoy instrument noise. Curves t_1 and t_2 show total errors to be expected with the two types of buoy winds.

with the AMI wind retrieval. Points on the a_1 curve that approach zero represent speeds at which multiples of the 10-minute time-averaged winds from the buoy exactly match the instantaneous spatial averages of AMI winds. Curve b represent errors due to AMI noise, and curve c to errors related to buoy instrument noise. Curves t_1 and t_2 show total errors to be expected with the two types of buoy winds. These figures indicate that, for an incidence angle of 40°, the accuracy specification of ± 2 m/s for AMI wind speed should be achieved for all winds below about 18 m/s with accuracies degrading with increasing wind speeds to about ± 2.8 m/s at 24 m/s. This degradation is due primarily to the effect of the AMI instrument noise (curve b) above 18 m/s.

Figure 2 illustrates AMI wind speed error dependence on beam incidence angle for a wind speed of 8 m/s. This shows the error increases with increasing angles of incidence due to the nature of the scatterometer model function. For winds at 24 m/s, the error at incidence angles near 15° can be as large as ± 3.6 m/s.

Figure 3 shows the AMI wind direction retrieval error dependence on direction of the wind relative to the beam direction for a wind speed of 8 m/s and a beam incidence angle of 40°. Errors are minimum for relative wind directions of about 45° and 135° but increase rapidly due to the decrease in slope of the model function as the slope approaches zero at 0°, 90°, and 180° where the errors are maximum. Errors in direction associated with the fixed and continuous buoy wind speeds are not shown since they are less than 0.5°.

Figure 4 presents the AMI wind direction error dependence on beam incidence angle for a wind speed of 8 m/s and a relative wind direction of 45°. Errors in direction increase with decreasing incidence angles and can be for winds of 24 m/s at incident angles of 15°.

Figure 5 shows AMI wind direction error dependence on wind speed for a wind direction of 45° relative to an AMI beam and for a beam incidence angle of 40°. This shows a very weak dependence on wind speed even at a relative wind direction of 45°, the worst case condition.

Figure 6 presents the wind speed dependence of the comparison error for the RA winds. Error totals are somewhat less than those calculated for AMI winds in Figure 1. These curves show that the accuracy specification of ± 2 m/s can be met for wind speeds below about 9 m/s and that accuracies degrade with increasing winds speeds to about ± 2.2 m/s at 15 m/s, the upper limit of the GEOSAT wind speed algorithm.

1.3 Data Requirements

For the analysis of cross-track bias, cell filling across the swath produced by the orbit patterns over the buoy network must be nearly equal. Figures 7, 8, and 9 present histograms of buoy locations within the 500 km swath at 10°, 40°, and 70° latitude, during the 3-day repeat cycle orbit based on a 60-day orbit simulation. Figures 10, 11, and 12 show the same information for the 35-day repeat cycle. These figures indicate that all cells in the 500 km swath will be nearly equally filled and that sufficient data will exist for an analysis.

The intersection of the RA nadir swath about a buoy location as a function of latitude
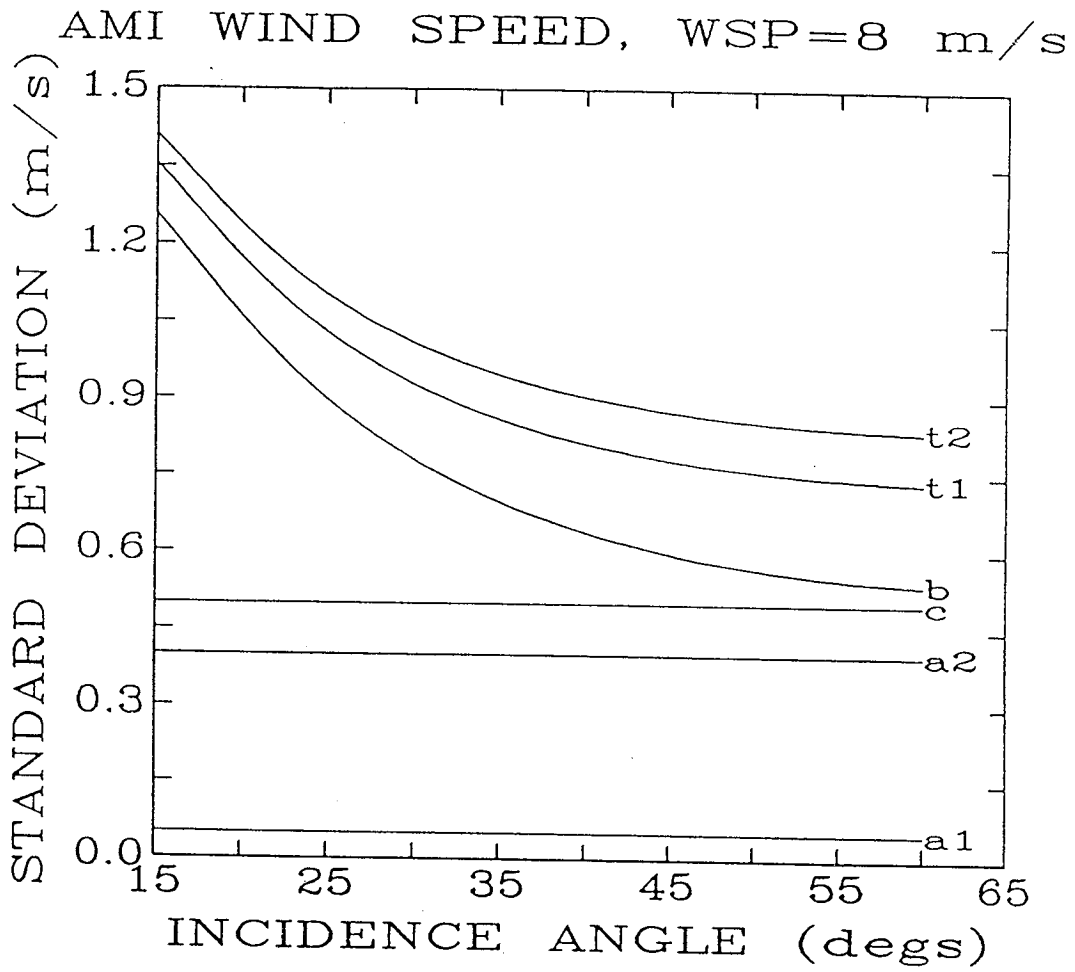
Figure 2. AMI wind speed error dependence on beam incidence angle for a wind speed of 8 m/s.
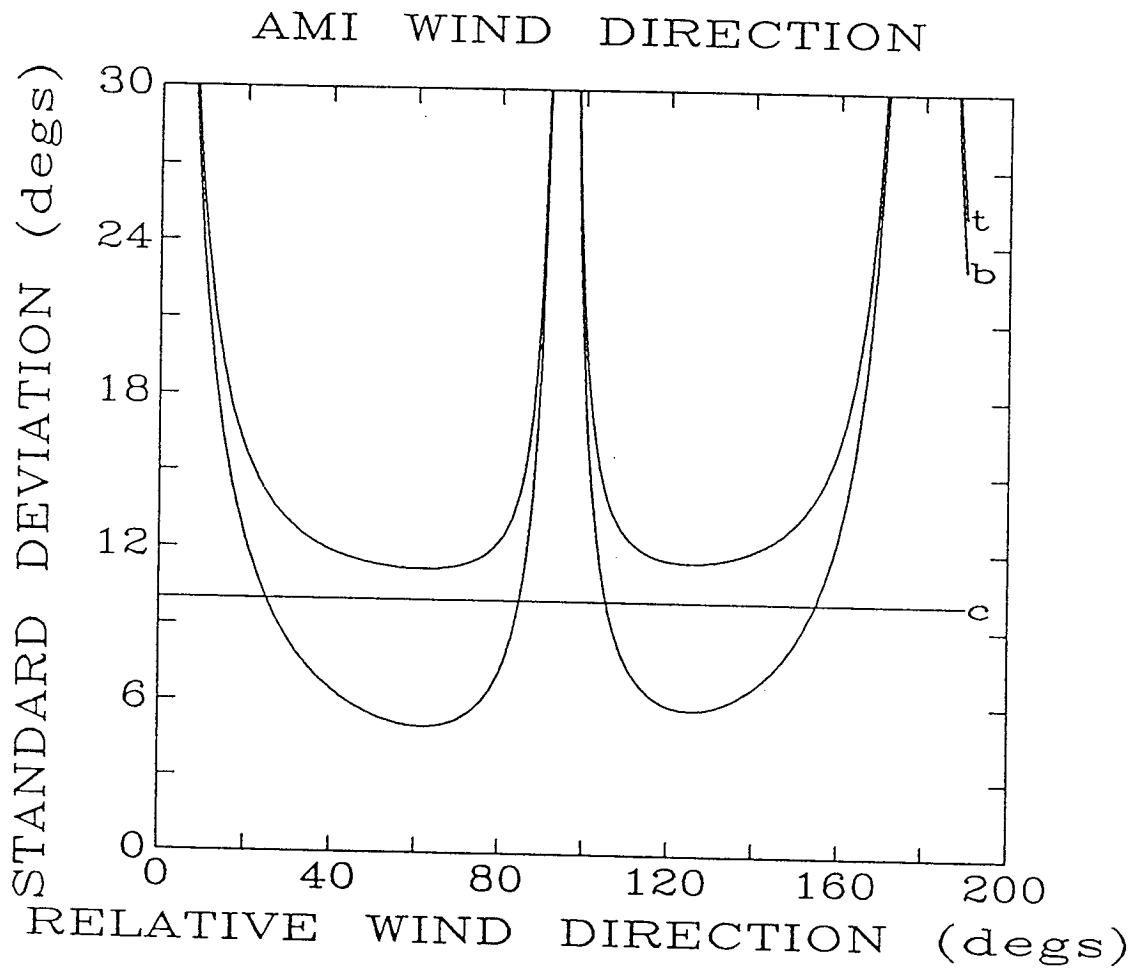
Figure 3. AMI wind direction retrieval error dependence on direction of the wind relative to beam direction for a wind speed of 8 m/s and a beam incidence angle of 40°. Errors are minimumfor relative wind directions of 45° and 135° but increase rapidly due to the decrease in slope of the model function as the slope approaches zero at 0°, 90°, and 180° where the errors are maximum.
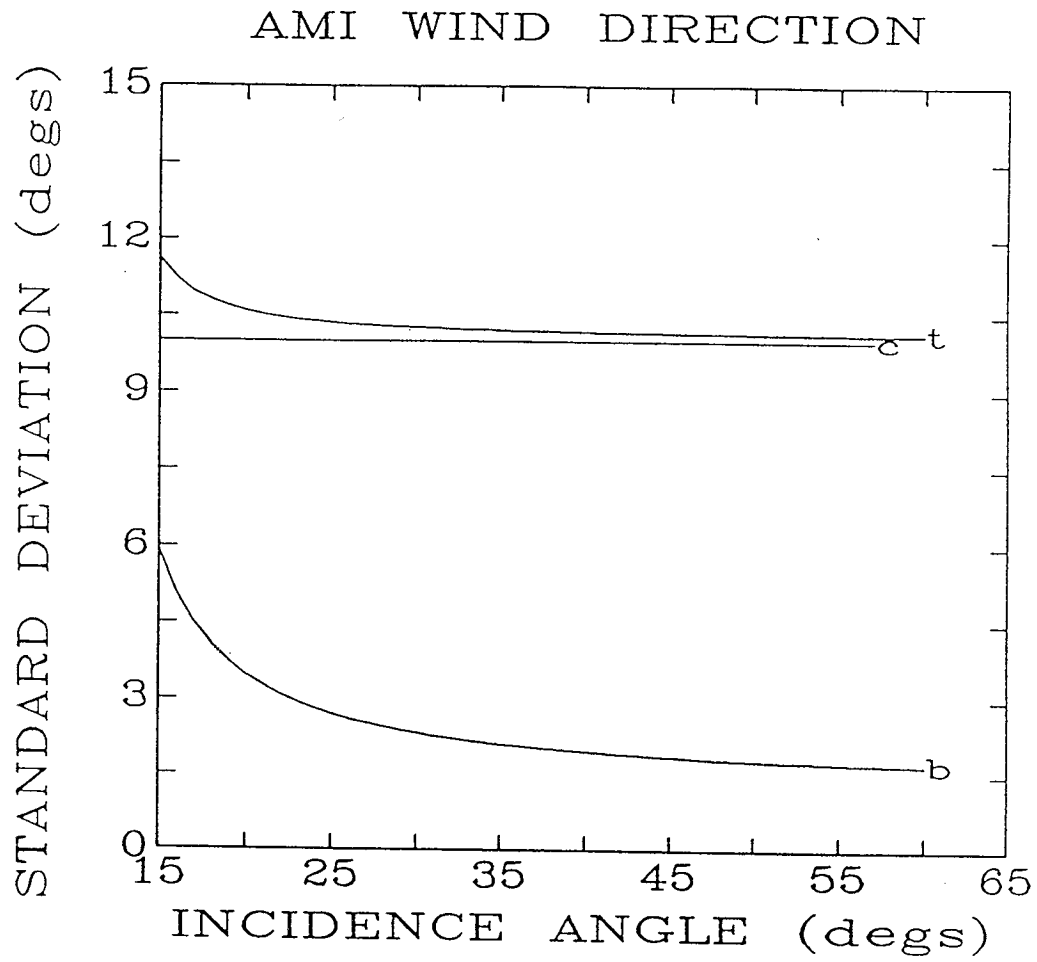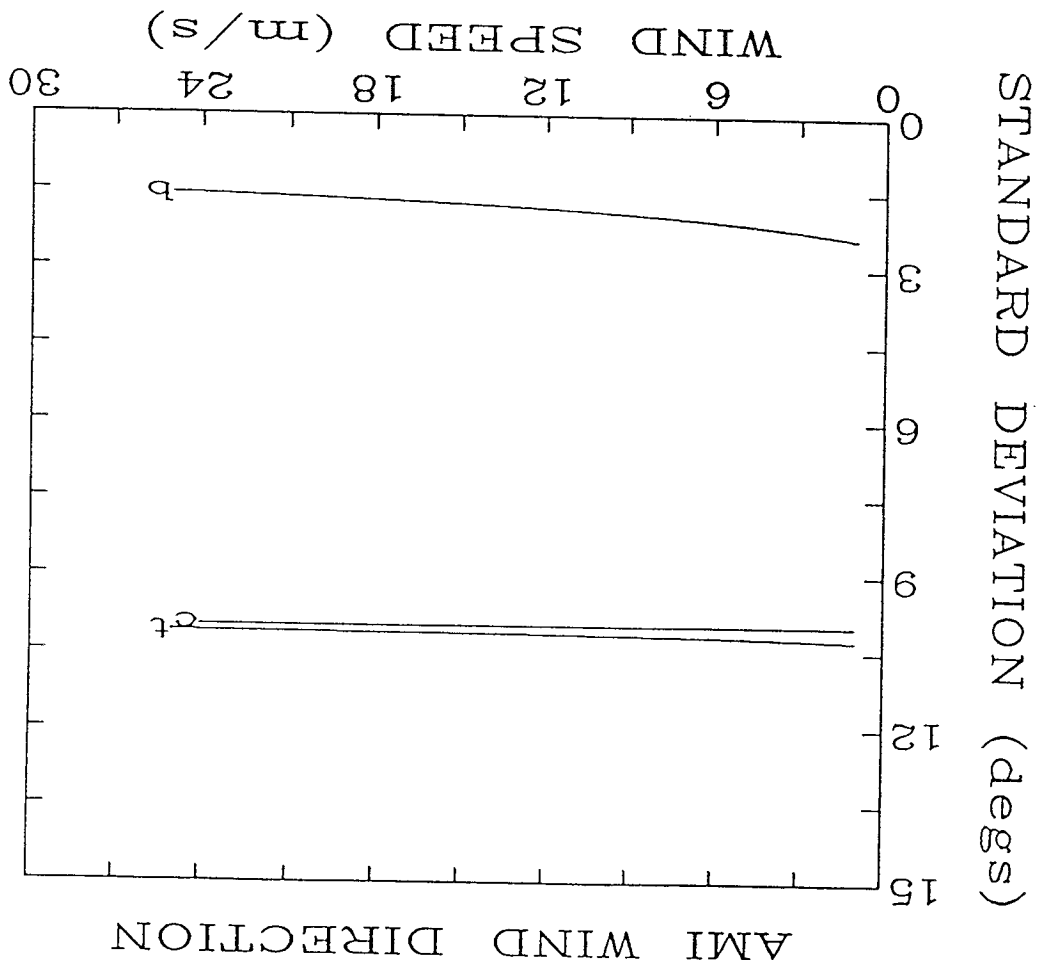
Figure 4. AMI wind direction error dependence on beam incidence angle for a wind speed of 8 m/s and a relative wind direction of 45°.

Figure 5. AMI wind direction error dependence on wind speed for a wind direction of 45° relative to an AMI beam and for a beam incidence angle of 40°.
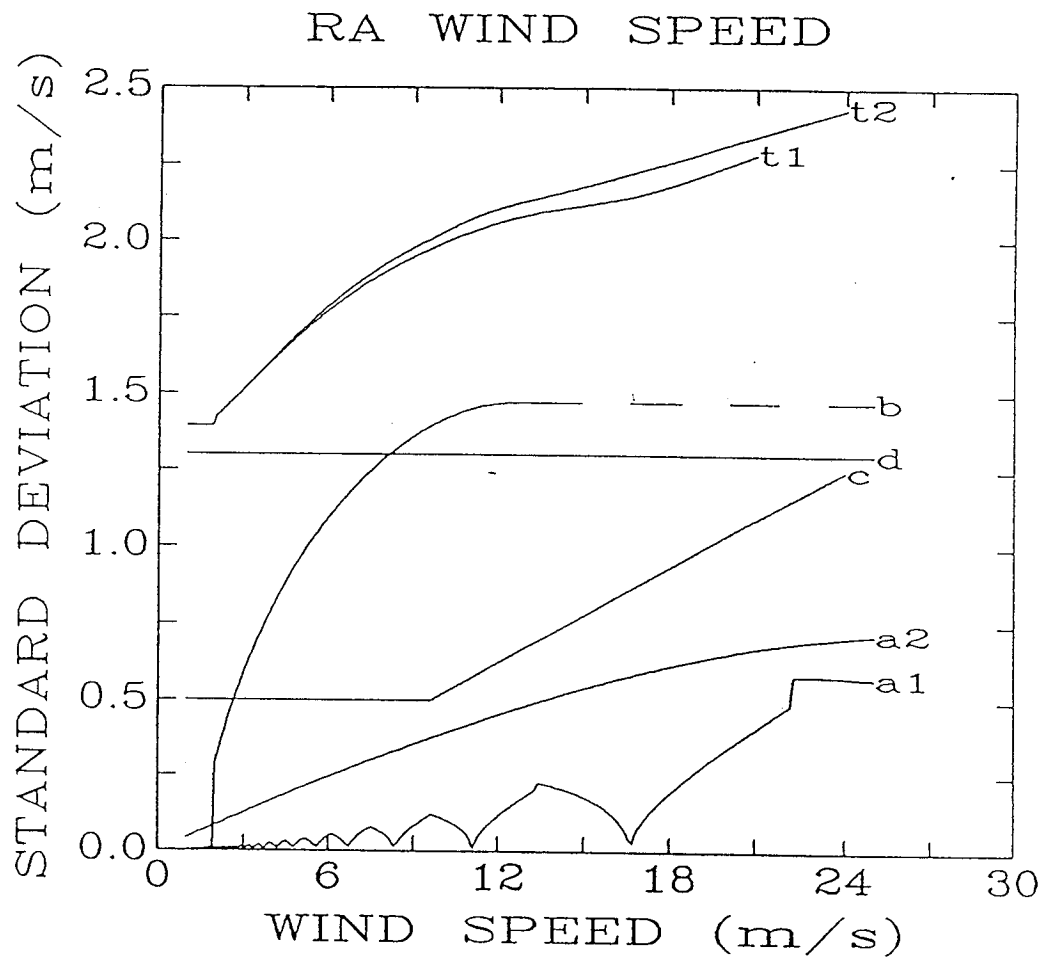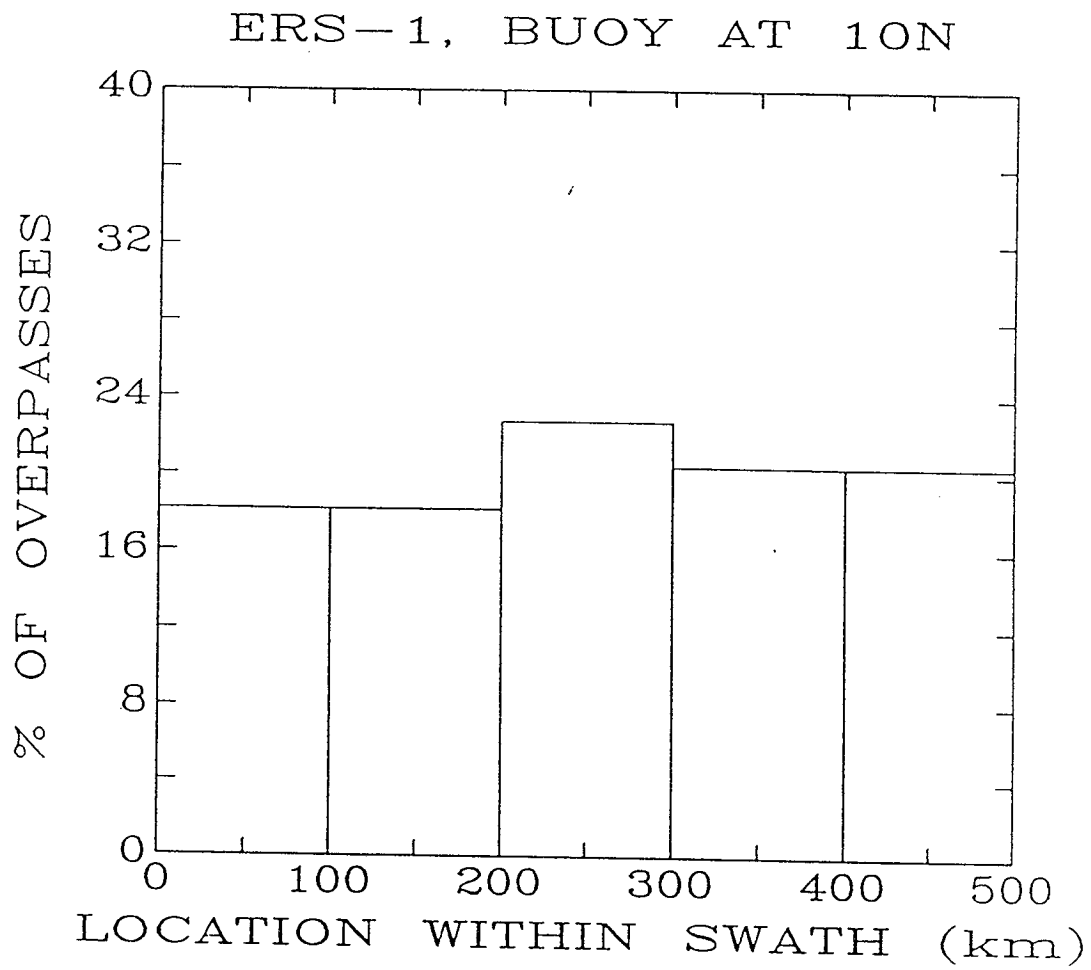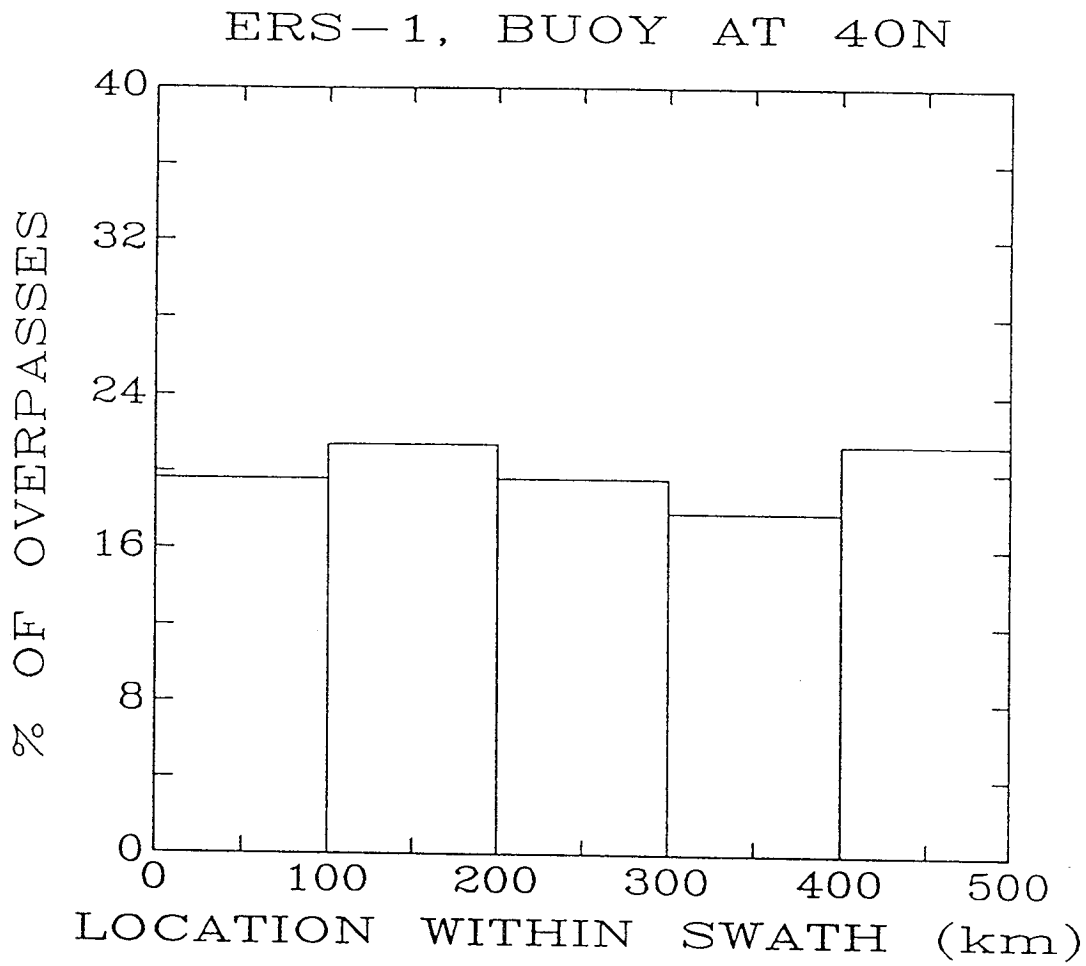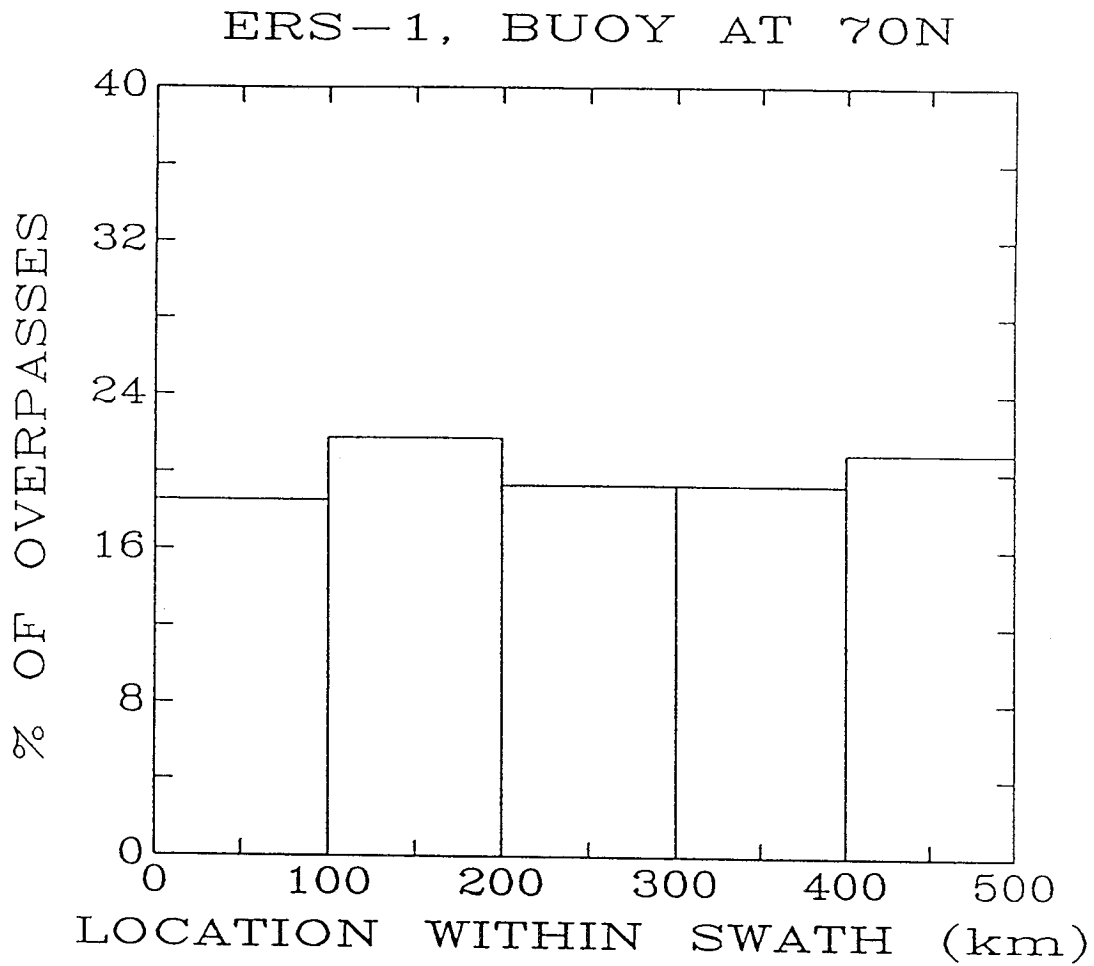
Figure 6. Wind speed dependence of the comparison error for the RA winds.

Figures 7. Histogram of buoy locations within the 500 km swath at 10°, for the 3-day repeat orbit cycle based on a 60 day simulation.

ERS-1, BUOY AT 40N

Figures 8. Histogram of buoy locations within the 500 km swath at 40°, for the 3-day repeat orbit cycle based on a 60 day simulation.

Figures 9. Histogram of buoy locations within the 500 km swath at 70°, for the 3-day repeat orbit cycle based on a 60 day simulation.
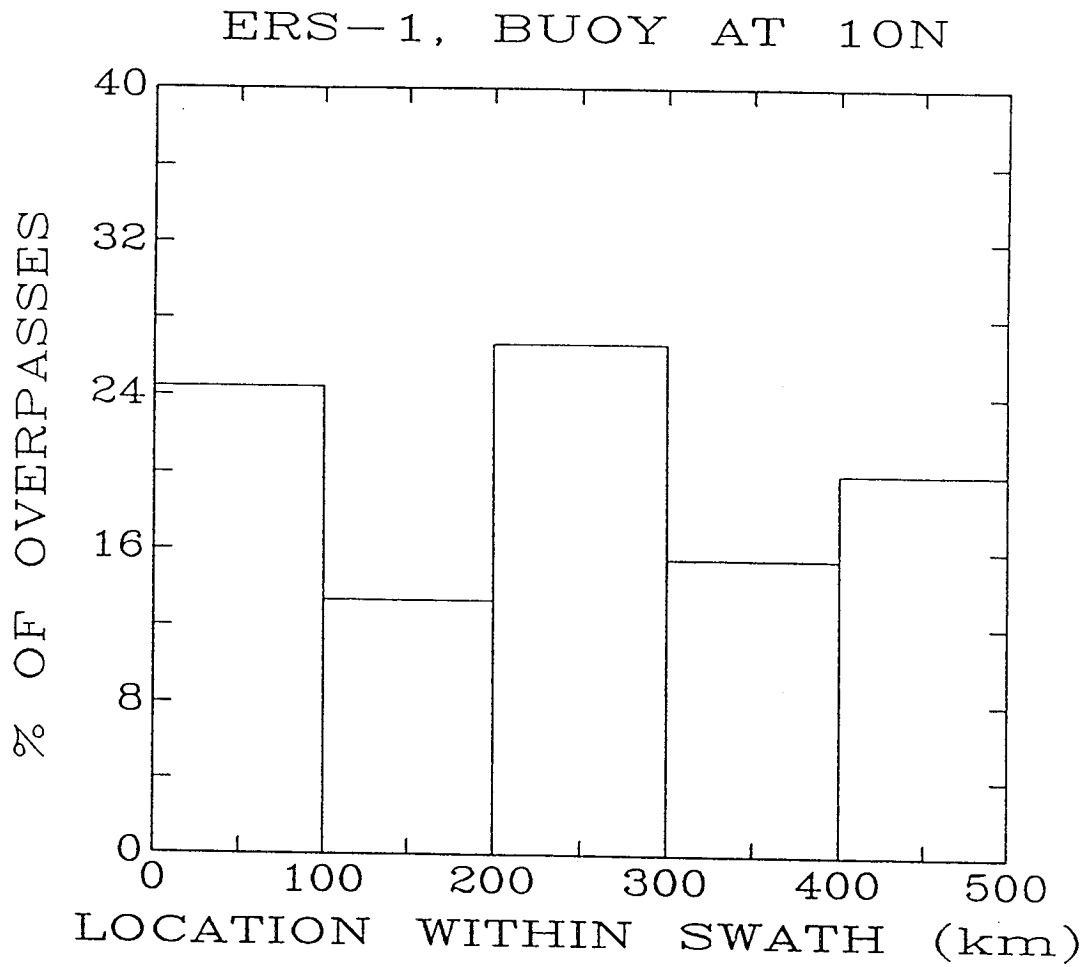
ERS-1, BUOY AT 10N

Figures 10. Histogram of buoy locations within the 500 km swath at 10°, for the 35-day repeat orbit cycle based on a 60 day simulation.
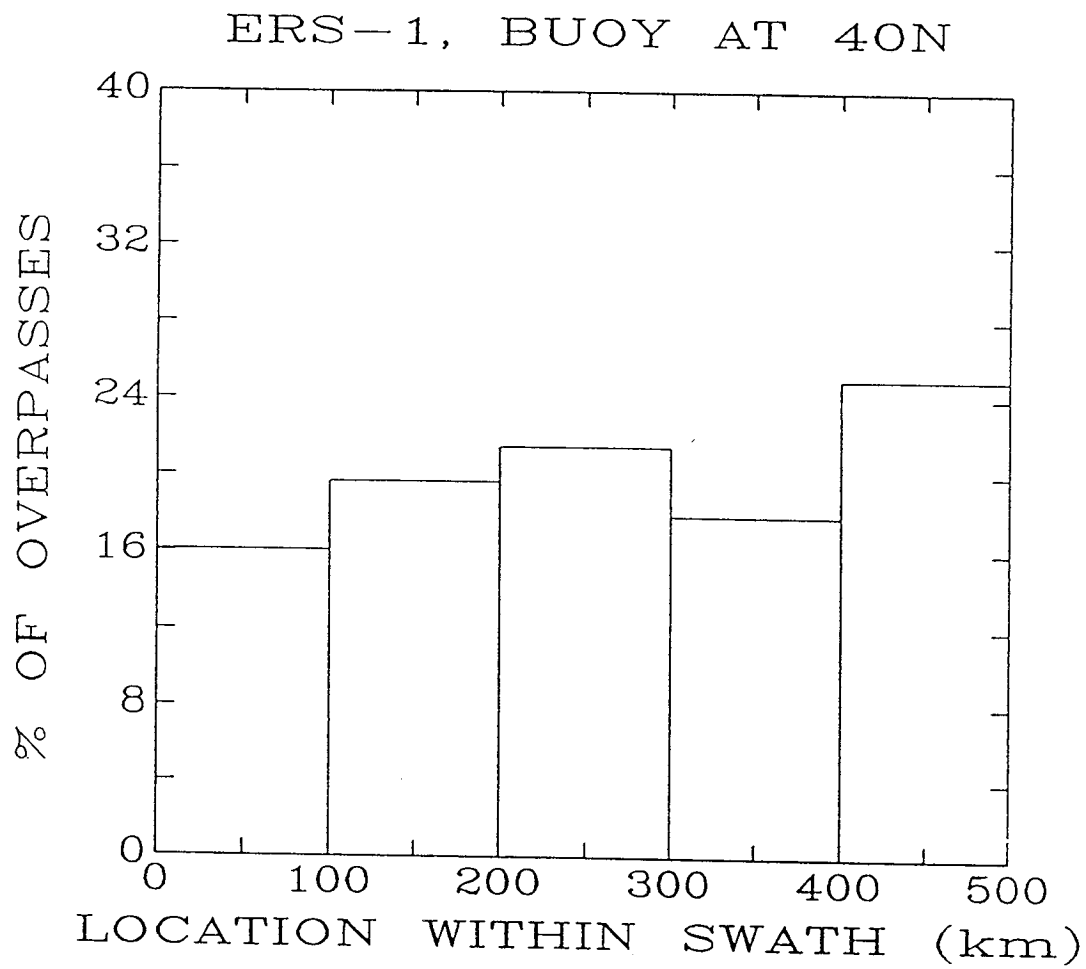
Figures 11. Histogram of buoy locations within the 500 km swath at 40°, for the 35-day repeat orbit cycle based on a 60 day simulation.
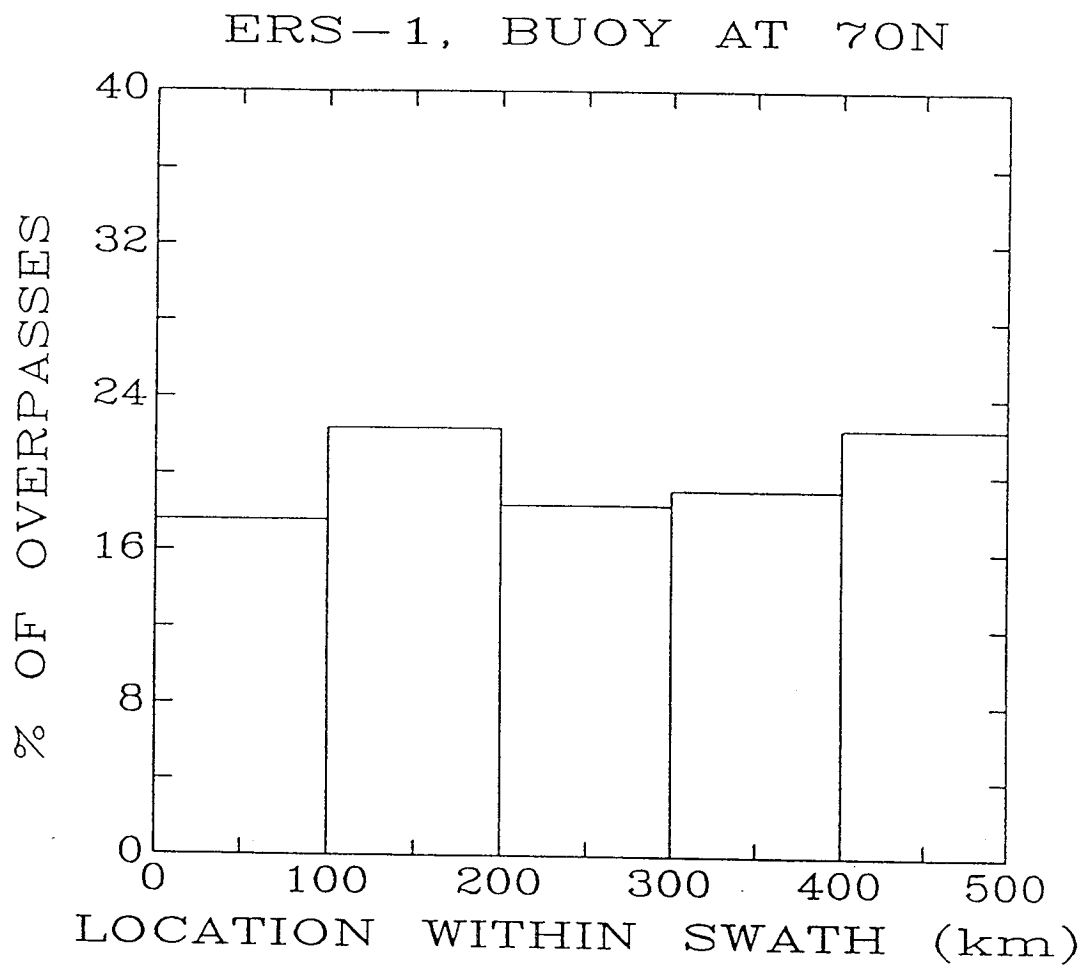
Figures 12. Histogram of buoy locations within the 500 km swath at 70°, for the 35-day repeat orbit cycle based on a 60 day simulation.

Gilhousen, D.B., An accuracy statement for meteorological measurements obtained from NDBC moored buoys, paper presented at MDS '86 Marine Data Systems International Symposium, Gulf Coast Sect., Mar. Technol. Soc., New Orleans, La, April 1986.

Gilhousen, D.B., M.J. Changery, R.G. Baldwin, T.R. Karl, and M.G. Burgin, Climatic summaries for NDBC data buoys, National Weather Service publication, 1986.

Long, A.E., Towards a C-band radar sea echo model for the ERS-1 scatterometer, ESA report WIND (version 1.01) Wind Retrieval and De-aliasing Subroutines, 1987.

Pierson, W.J., Jr., The measurement of synoptic scale wind over the ocean, *J. Geophys. Res.*, Vol 88, C3, 1683-1708, 1983.

is shown in Figures 13 and 14 for the 3-day and 35-day repeat cycle orbits. These Figures indicate that buoys at about 50°N will be within 150 km of nadir once every three days for both orbit cycles with coverage increasing to once per day near 50°N. During the 35-day repeat cycle, areas below 50°N will be within range about once every 4 days. Because of the nadir-only coverage of the RA, data buildup for the verification of RA winds and significant wave height will be much slower than for the AMI and ATSR. The rate of data collection over a 90-day period, for the select network of buoys, is shown in Table 1 for all instruments.

The number of satellite/buoy data pairs required for verification can be determined from Figure 15 which shows the sample size dependence of the upper and lower limits on the 90% confidence interval for estimating standard deviation. This example shows that for a true standard deviation of 2, sample sizes larger than 30 do not significantly reduce the size of the confidence interval. Therefore, a sample size of 30 will give a good estimate of standard deviation. If for wind speed, the range of 4-24 m/s is divided into five bins, the number of days required to fill each range bin can be determined using the data of Figure 15 and the annual distribution of wind speeds for the buoy network, Figure 16, taken from *Gilhousen et al., [1986]*. The results of the calculations are shown in Table 2. Tables 3 and 4 present the results of similar calculations for significant wave height and sea surface temperature using Figures 17 and 18, the annual distributions of these parameter for the buoy network.

Because of the very low probability of the occurrences of high winds and waves from the buoys, the range bins for wind speeds above 16 m/s and for significant wave heights above 8 m will have less than the required sample size of 30. In the case of winds, this data shortage is expected to be filled with data from the stepped-frequency microwave radiometer in flights of NOAA aircraft during the hurricane season.

When the remaining error structure analyses for the RA significant wave height and ATSR sea surface temperature have been conducted, NOAA pre-launch test activity for the fast delivery products will have been completed. The pre-launch activity relating to validation of the sea level measurements from RA height data, to be carried out within National Ocean Service (NOS) is nearing completion with the procurement of additional processing hardware.

REFERENCES

Applications and Scientific Uses of ERS-1 Radar Altimeter Data, ESA contract report under ESTEC contract No. 5684/83/NL/BI,1985.

Carter, D.J.Q., ERS-1 wind scatterometer system design, published by the Marconi Company Limited, 1990.

Dobson, E., F. Monaldo, J. Goldhirsh, and J. Wilkerson, Validation of Geosat altimeter-derived winds speeds and significant wave heights using buoy data, *J. Geophys. Res.*, vol. 92, C10, 10,719-10,731, 1987.

TABLE 1. Rate of validation data collection over a 90-day period for the select network of buoys according to instrument.

Number of Buoy Overflights for ERS-1 Instruments During a 90 Day Period

(8.5–minute average buoys as of 6 Aug 1990)

Buoy I.D.	Latitude	Longitude (E)	AMI, ATSR	RA
51002	17.2	202.2	36	23
51004	17.5	207.4	36	23
51003	19.2	199.2	36	23
51001	23.4	197.7	37	24
41002	32.2	284.7	40	25
46005	46.1	229.0	46	28
90–Day Total			231	146

(10–minute consecutive average buoys as of 6 Aug 1990)

Buoy I.D.	Latitude	Longitude (E)	AMI, ATSR	RA
42001	25.9	270.3	38	24
42002	26.0	266.5	38	24
42003	26.0	274.1	38	24
41006	29.3	282.6	39	25
44004	38.5	289.4	41	27
46006	40.8	222.4	41	27
44011	41.1	293.4	42	27
46002	42.5	229.6	43	28
44005	42.7	291.7	43	28
46003	51.9	204.1	50	30
46001	56.3	211.7	56	32
46035	57.0	182.3	59	33
90–Day Total			528	329

Yearly Totals

AMI, ATSR —— 3078

RA ———— 1931

TABLE 2. Number of days to collect 30 data pairs per wind speed range bin.

WIND SPEED VALIDATION
(Number of days to collect 30 hits per bin)

Bin Range (m/s)	Days(*) for AMI	Days(*) for RA
4–8	9	14
8–12	17	27
12–16	88	140
16–20	631	1009
20–24	∞	∞

(*) 10 percent added to account for lost data

TABLE 3. Number of days to collect 30 data pairs per wave height range bin.

WAVE HEIGHT VALIDATION
(Number of days to collect 30 hits per bin)

Bin Range (m)	Days(*) for RA
0–4	8
4–8	69
8–12	3127
12–16	∞
16–20	∞

(*) 10 percent added to account for lost data

TABLE 4. Number of days to collect 30 data pairs per sea surface temperature range bin.

SEA TEMPERATURE VALIDATION
(Number of days to collect 30 hits per bin)

Bin Range (C)	Days(*) for ATSR
3–9	18
9–15	13
15–21	32
21–27	26
27–33	21

(*) 10 percent added to account for lost data
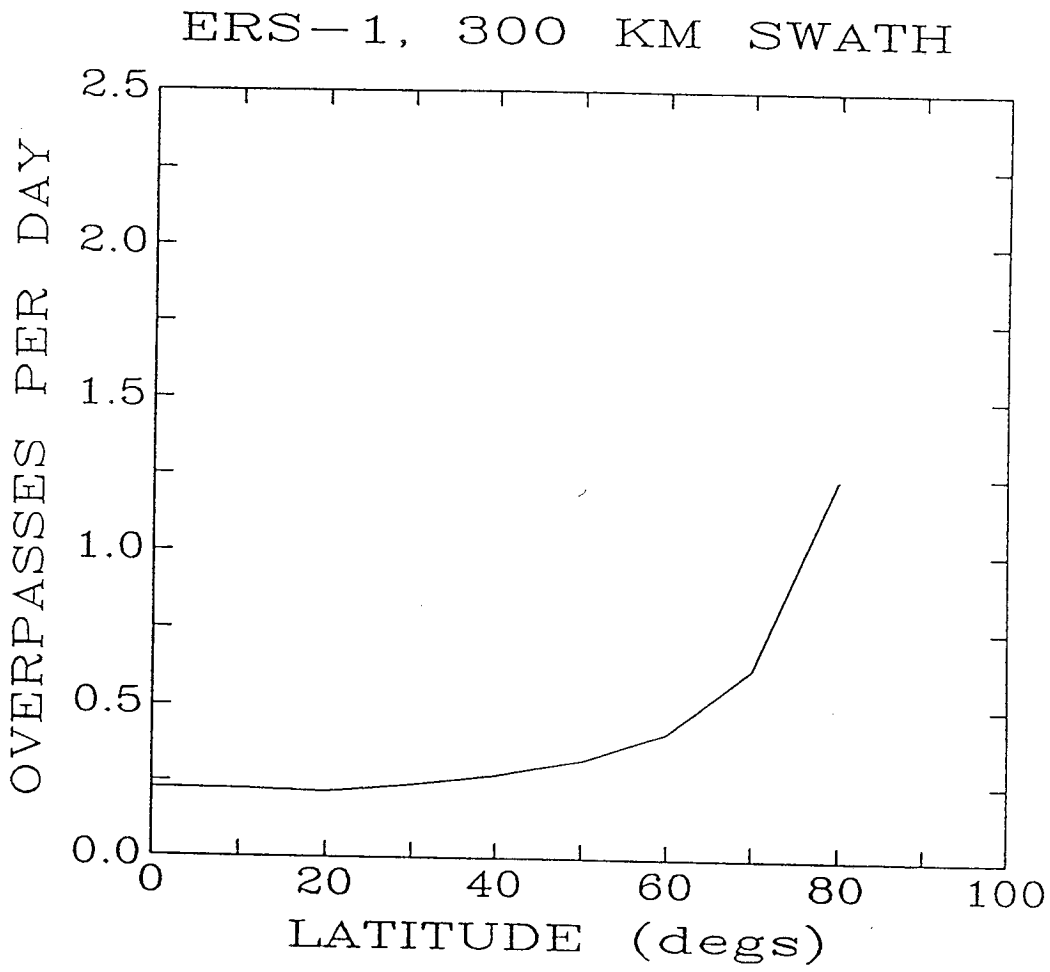
ERS-1, 300 KM SWATH

Figure 13. Intersersection of the RA nadir swath with an area of 150 km radius, centered on buoy locations as a function of latitude. Simulation is based on a 60-day run of the 3-day repeat cycle.
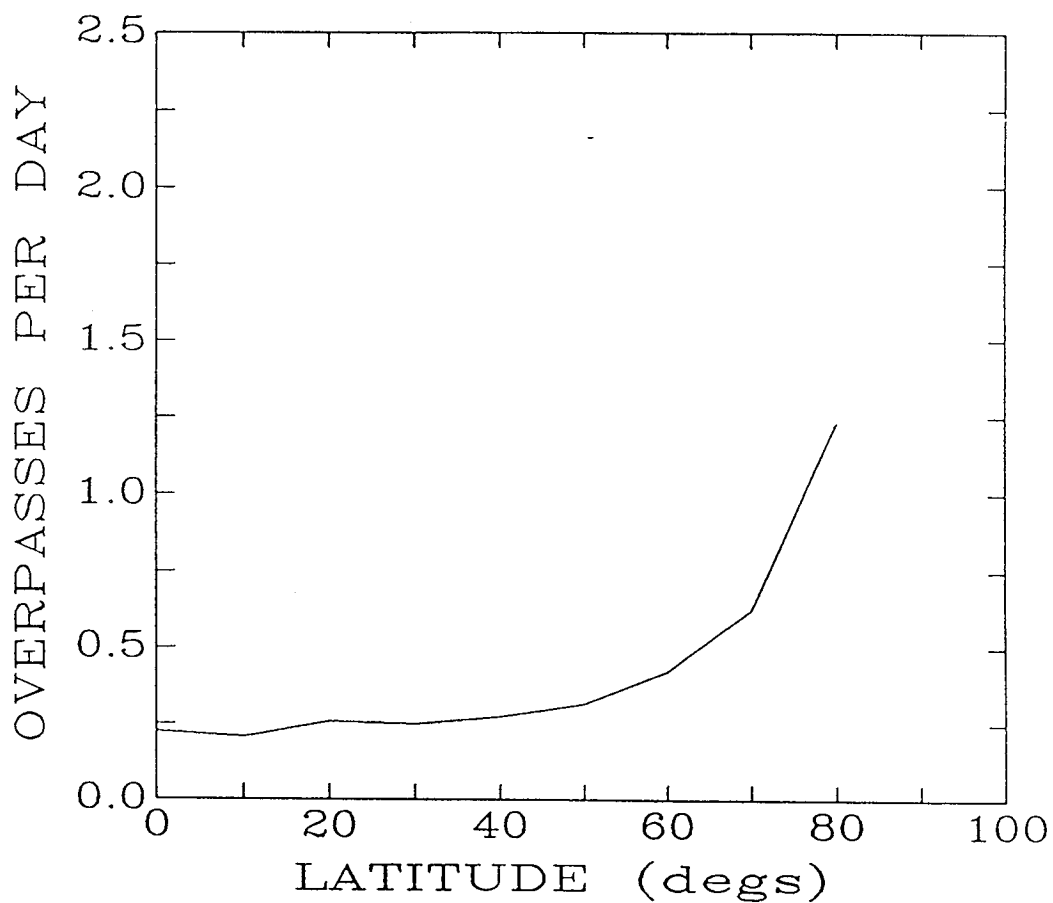
Figure 14. Intersersection of the RA nadir swath with an area of 150 km radius, centered on buoy locations as a function of latitude. Simulation is based on a 60-day run of the 35-day repeat cycle.
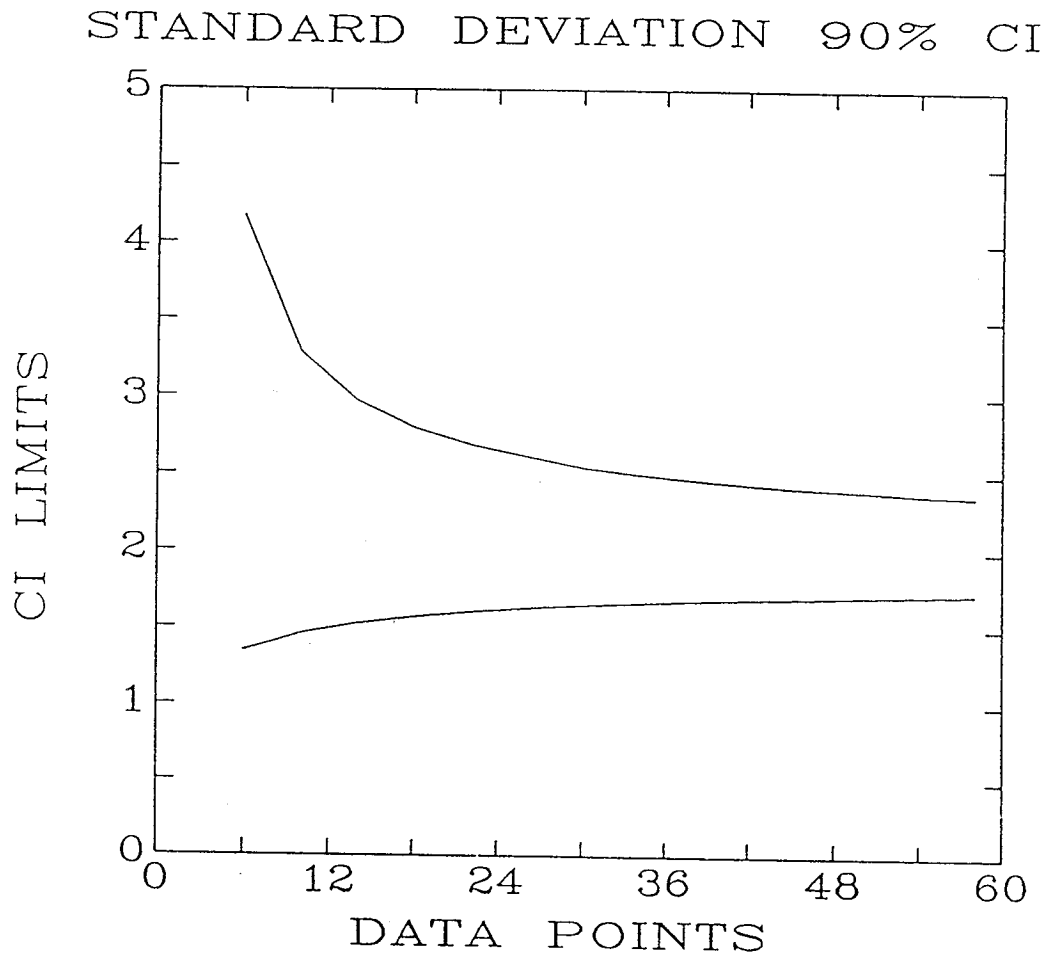
STANDARD DEVIATION 90% CI

Figure 15. Sample size dependence of the upper and lower limits on the 90% confidence interval for estimating standard deviation. For a true standard deviation of 2, sample sizes larger than 30 do not significantly reduce the size of the confidence interval. Therefore, a sample size of 30 will give a good estimate of the standard deviation.
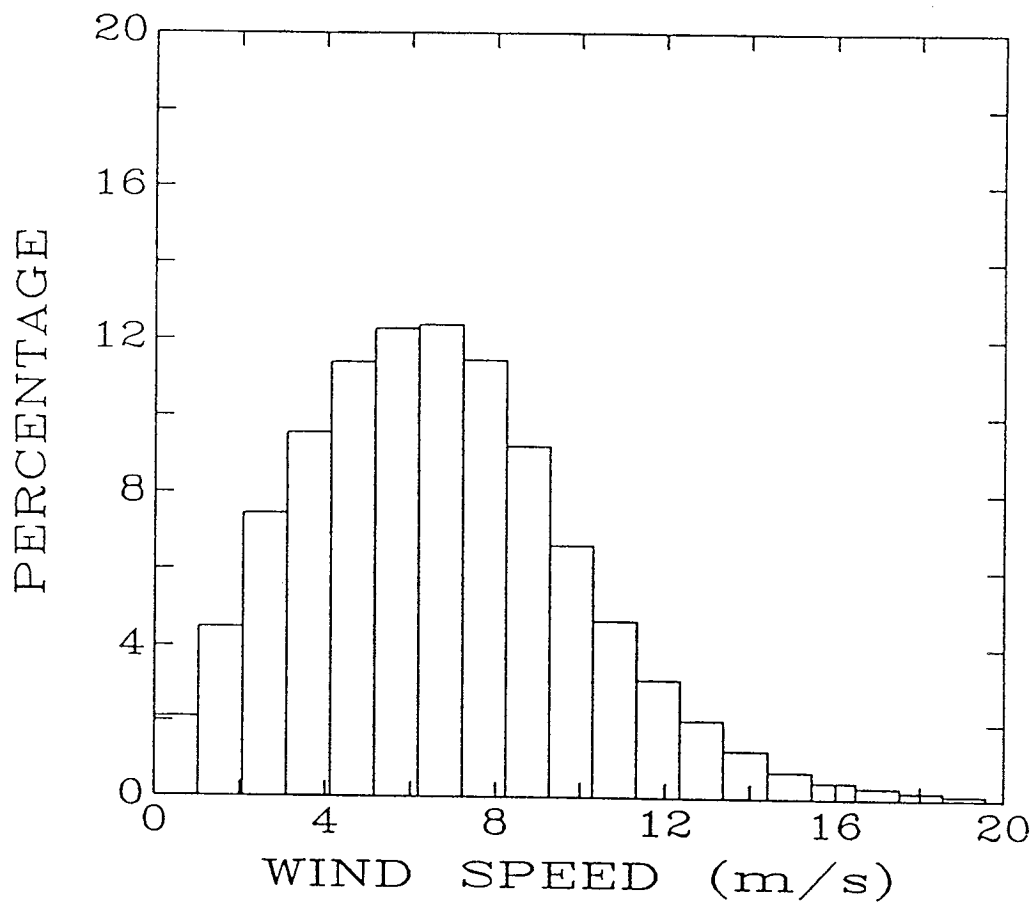
Figure 16. The annual distribution of wind speeds for the buoy network from climatological summaries.
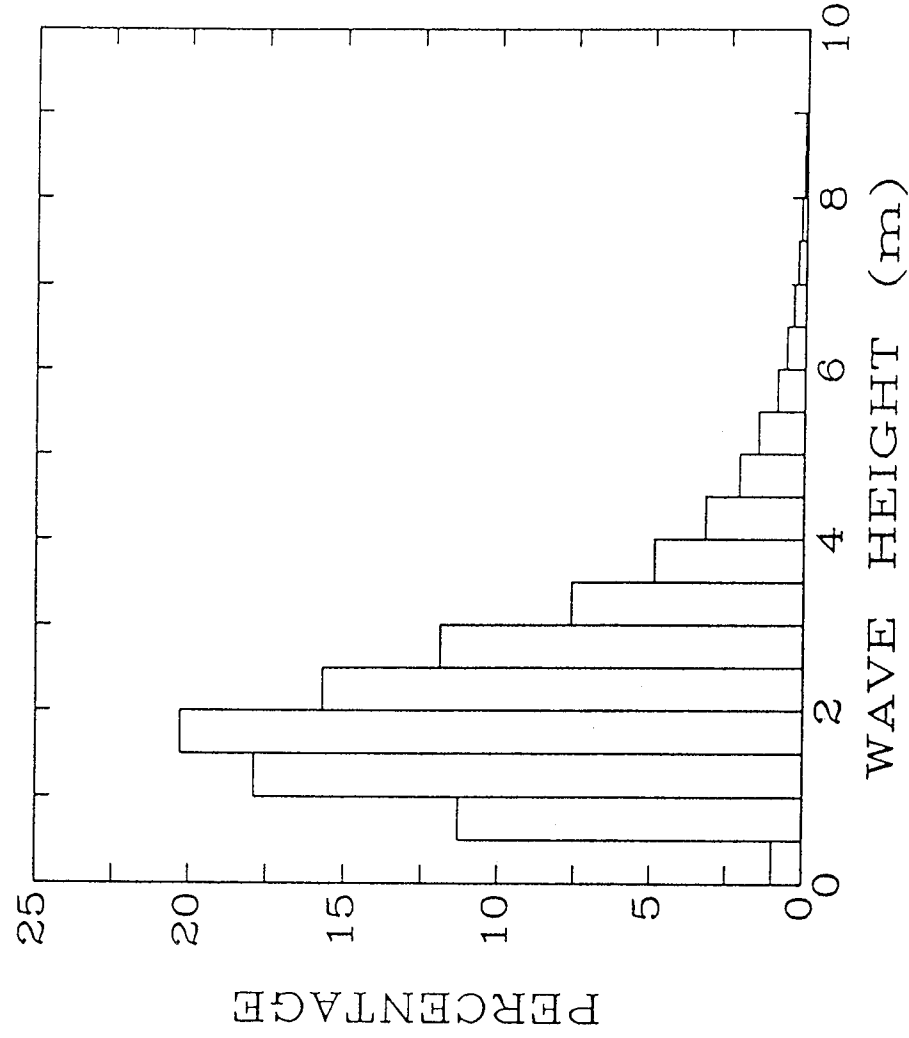
Figure 17. The annual distribution of significant wave height for the buoy network from climatological summaries.
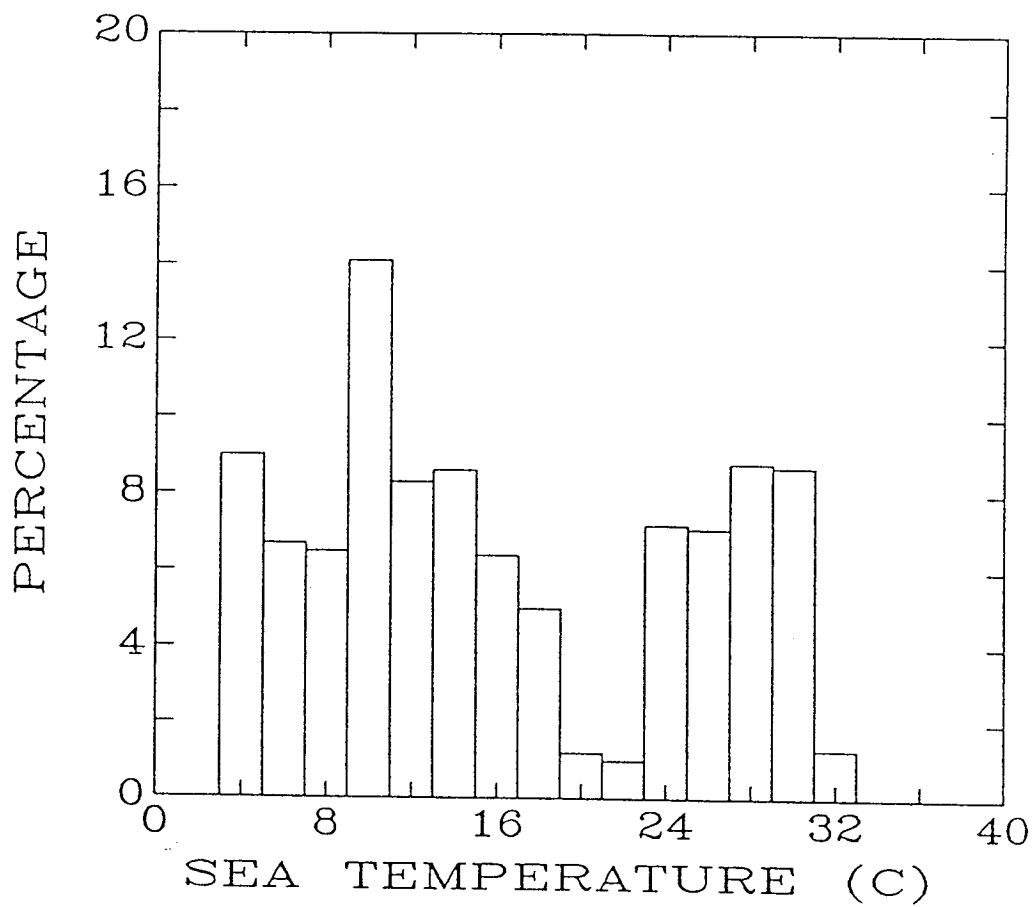
Figure 18. The annual distribution of sea surface temperature for the buoy network from climatological summaries.

Chapter 2
Validation Results

2.1 Introduction

Validation of environmental algorithms used to retrieve ERS–1 estimates of over–ocean wind vectors from the Active Microwave Instrument (AMI) and wind speeds and significant wave heights from the Radar Altimeter (RA) was done by comparing those derived environmental parameters with measurements of the same made by 24 of the open ocean buoys maintained by the National Oceanic and Atmospheric Administration (NOAA) The buoys are of two basic types; standard buoys which make an 8.5–minute average of the wind once every hour and continuous–average buoys which make six consecutive 10–minute averages of the wind each hour. Buoy wind measurement accuracy for both buoy types is reported in *Gilhousen [1990]* to be ±0.5 m/s for winds less than 10 m/s and ±5% for winds greater 10 m/s. Buoy wind direction measurement accuracy is reported to be ±10°. Both types of buoys measure the ocean significant wave height using a 20–minute average once every hour with a reported accuracy of ±0.2 m. To prevent land contamination of the over–ocean AMI and RA backscatter measurements and to insure that land did not restrict the wind fetch distance necessary for creating fully developed seas, only buoys further than 90 km from land were chosen for the validation. See Table 5 for the list of buoys used in this study.

2.2 Method of Comparison

Comparisons of ERS–1 wind estimates with those from the buoys was done in accordance with the following criteria. All buoy wind speeds were converted to a reference level of 10 m using the ESA supplied FORTRAN computer software called UREF v1.01 described by *Ezraty [1985]*. Converted buoy winds and ERS–1 winds were paired only when the ERS–1 retrieval was both within a 200 km (for AMI) or 400 km (for RA) radius of the buoy and was further than 50 km from land. Only the single AMI and RA wind retrieval from each ERS–1 overpass which was closest in distance to the buoy was retained for inclusion in the data base. Since the average wind field could change as a function of distance from the buoy, the comparison error between sensor and buoy measurements can be expected to increase with increasing separation distance. It was therefore desirable to keep the separation distance small enough so as not to affect the comparison error but, at the same time, keep it large enough to collect a sufficient number of comparisons. This decision was especially critical for the RA validation. The information in Figure 19 is given as partial justification for a 400 km comparison window. This plot indicates that for the data used in this analysis there was no significant increase in comparison error between RA and buoy measurements of wave height and wind speed for separation distances up to 400 km.

To minimize the error resulting from comparisons of point measurements at the buoys with spatial averages from the satellite, it is necessary to insure equivalence of measurement by selecting the correct averaging time for the point measurement of the buoy. To this end, a vector average (for AMI) or scalar average (for RA) of the buoy measured winds

Table 5. Location of the 24 NOAA buoys used in the validation. "Alt" is the buoy anemometer height. "Dist" is the buoy's approximate distance from land. (*) beside the buoy I.D. indicates a continuous average type buoy.

I.D.	Lat	Lon(E)	Alt(m)	Dist(km)
32302	-18.00	274.90	5.0	1010
*41001	34.89	287.14	5.0	240
41002	32.29	284.76	5.0	310
*41006	29.30	282.62	5.0	320
41010	28.88	281.47	10.0	180
*42001	25.93	270.35	10.0	330
*42002	25.93	266.41	10.0	350
*42003	25.94	274.09	10.0	380
42019	27.90	265.00	5.0	110
*44004	38.50	289.36	5.0	300
*44005	42.65	291.44	5.0	165
*44011	41.08	293.42	5.0	280
44014	36.58	285.17	4.0	90
44026	36.02	286.52	5.0	180
*46001	56.30	211.70	5.0	270
*46002	42.53	229.61	5.0	460
*46003	51.85	204.08	5.0	370
46005	46.08	229.00	5.0	500
*46006	40.81	222.35	10.0	1100
*46035	56.96	182.27	10.0	400
51001	23.42	197.66	5.0	220
51002	17.16	202.18	5.0	250
51003	19.18	199.18	5.0	360
51004	17.43	207.49	5.0	270

Figure 19. Cumulative histogram of the distance for RA measurements from the NOAA buoys. Dashed-line plots labelled WS and WV indicate the dependence of the RMS difference between RA and buoy measurements of wind speed (m/s) and wave height (m) upon the RA measurement distance from the buoy. The cause of the pronounced increase in RMS difference in WS with distance between 90 and 220 km is unknown.
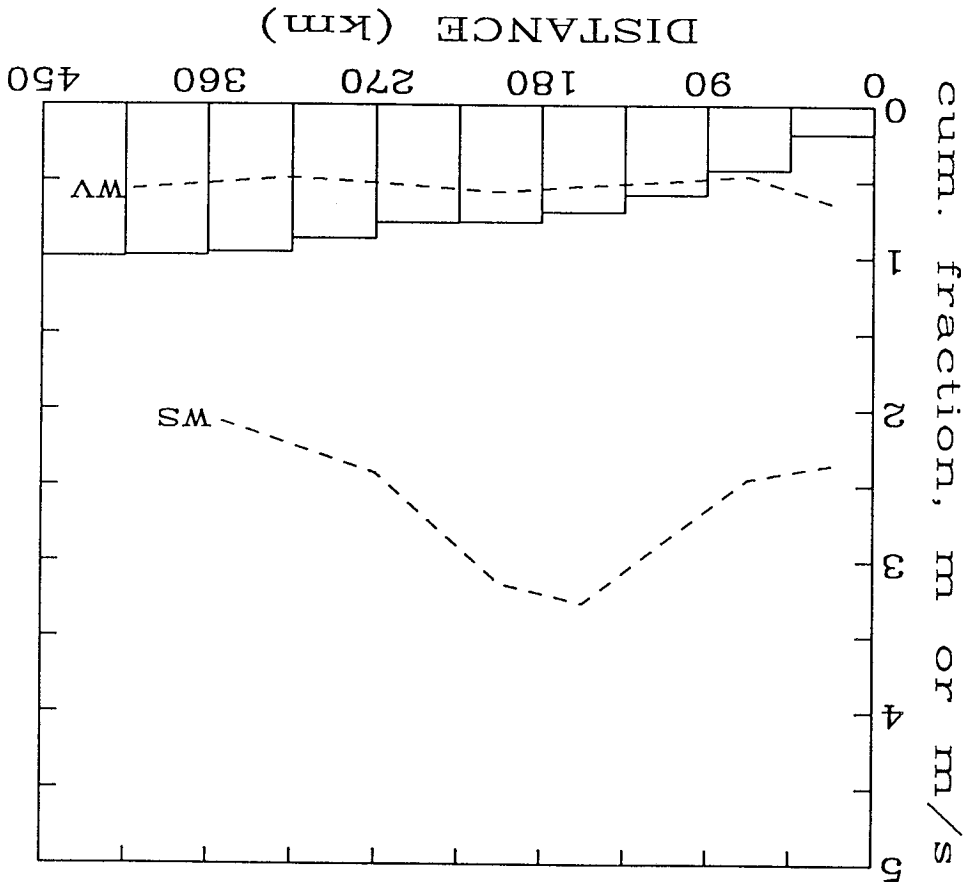
in a time interval, T, centered on the ERS–1 overpass time was used for comparison with the ERS–1 wind speed retrievals. *Pierson [1983]* suggests that when T is chosen to equal the sensor resolution cell diameter divided by the wind speed then "the averaging effect" is approximately the same for the buoy time series average and the satellite sensor spatial average. The resolution cell size for the AMI and RA is approximately 50 km and 18 km respectively. The Pierson averaging time for a buoy comparison with each of these instruments is plotted in Figure 20 as a function of wind speed. Careful application of the Pierson averaging technique is necessary since for large values of T one is likely to observe true changes in the average wind field in addition to random fluctuations about a constant wind field. As a result, the comparison error may actually increase for values of T which are too large. For this reason, T was not allowed to exceed 1 hour even when longer averaging times were specified. Errors associated with the current ERS–1 retrieval algorithms (especially for the AMI) appear to dominate the comparison error budget. Therefore, the small changes in the total comparison error resulting from the Pierson averaging can not be seen. The full effect of this technique should be apparent in later analysis when improved environmental algorithms are implemented. The comparison criteria for ocean wave estimates is similar to that for winds except that the UREF software does not apply and only the buoy measurement closest in time to the ERS–1 overpass is used.

This work is based on ERS–1 measurements made after November 1, 1991 which marked the conclusion of the engineering calibration and system check–out phase for the ERS–1 sensors. However, during the validation phase that followed, launch versions of the retrieval algorithms were revised several times. Therefore, the retrieval accuracy estimates resulting from this study represent the combined performance of several versions of each algorithm and can only be considered tentative. A final assessment will be conducted when ESA completes current work on algorithm and model function improvement.

Using data collected during the period from November 1, 1991 to February 28, 1992, and the procedure described above, 1147 AMI/buoy coincident pairs were formed with only 577 being useful for validating AMI wind products. The balance of the 1147 coincident pairs had to be discarded because the AMI wind algorithm reported a default value of wind speed (an indication that the algorithm was unable or not allowed, as discussed below, to report estimates of wind speed and wind direction). A total of 485 coincident pairs were acquired for validating RA wind and wave products.

2.3 Analysis and Results

In the discussion that follows, "bias" refers to the average value of the quantity, (algorithm retrieval minus buoy measurement), and standard deviation, SD, refers to the root–mean–square value of the same quantity. Bias will be used to quantify the amount by which the ESA algorithms either underpredict or overpredict the true value of the environmental parameter. The SD is used to quantify the random error associated with the retrievals.

The histogram shown in Figures 21 and 22 indicates the range and distribution of
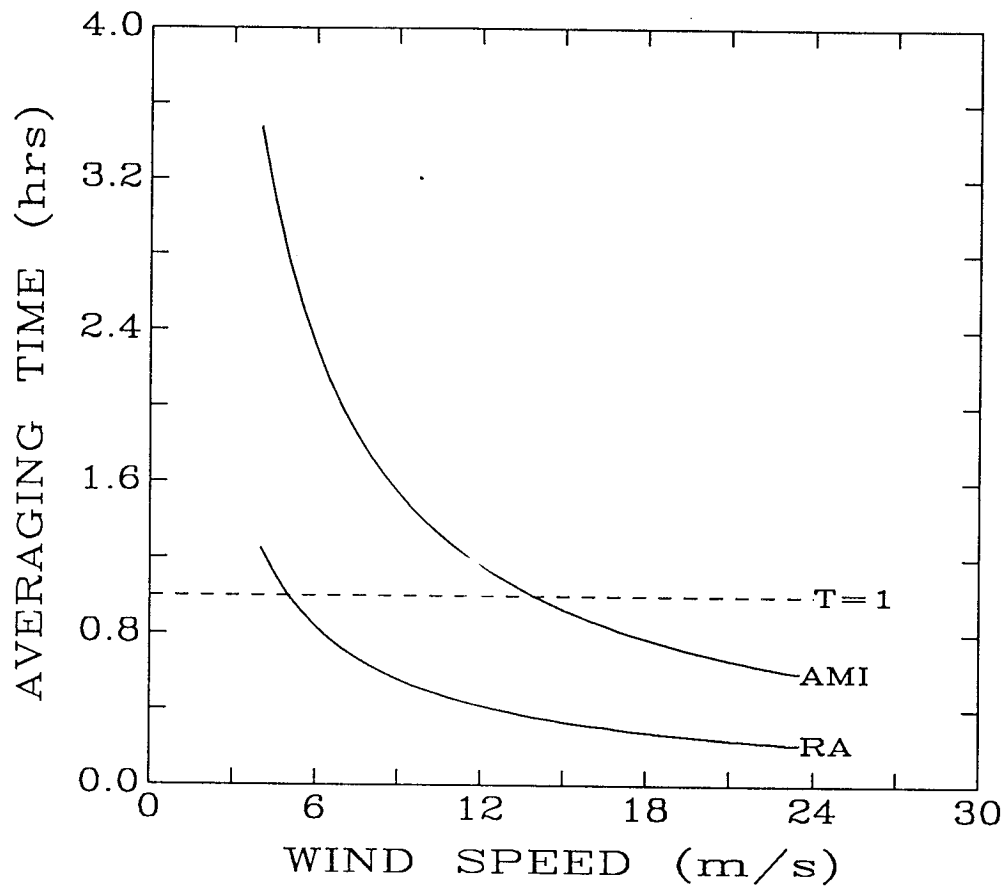
Figure 20. Pierson averaging time used to compare buoy measurements of wind speed to retrievals of the AMI and RA for the AMI measurement range of 4-24 m/s and the RA range of 4-15 m/s.
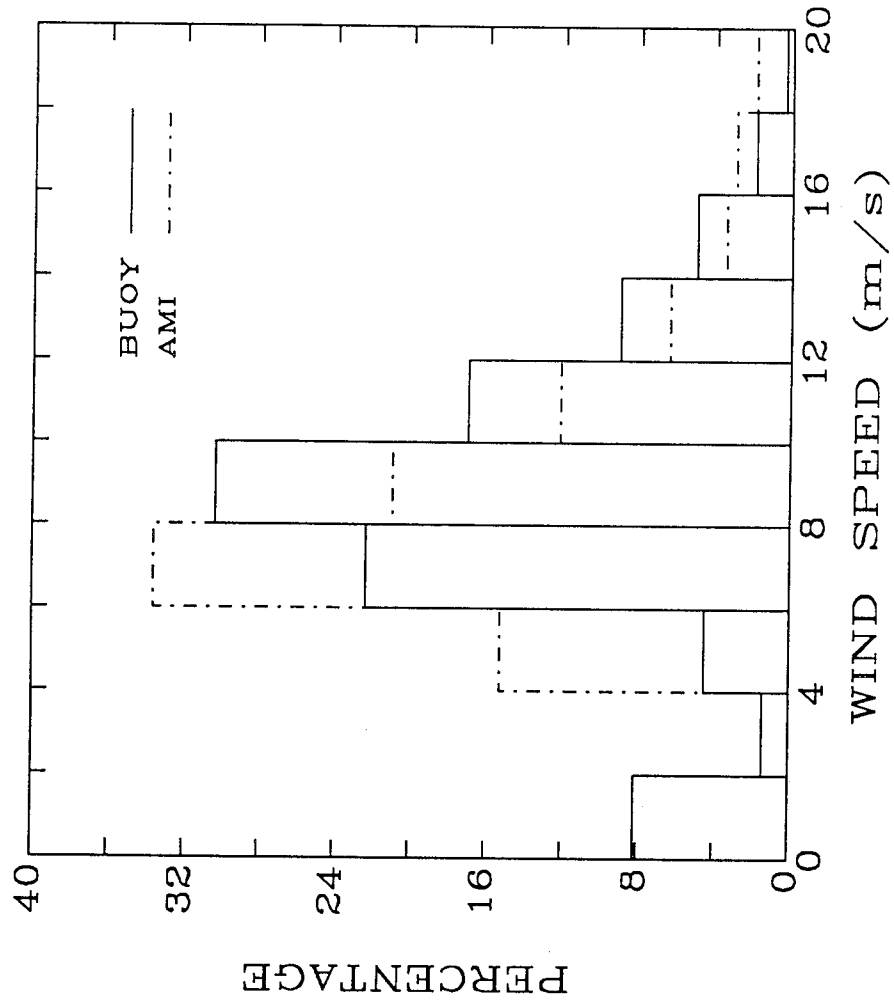
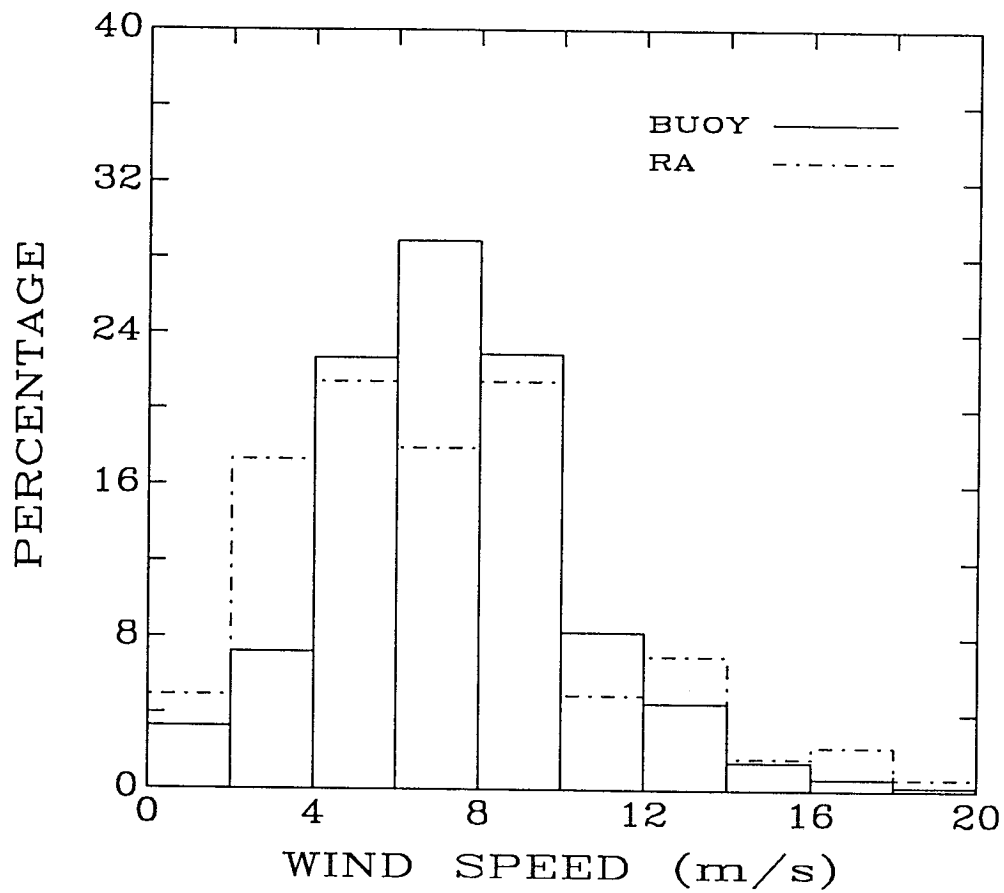Figure 21. Distribution of buoy (solid line) and coincident AMI (dot-dash line) retrieved wind speed.

Figure 22. Distribution of buoy (solid line) and coincident RA (dot-dash line) retrieved wind speed.

wind speeds found in the AMI and RA coincident pair data sets. Each figure contains two histograms; one for the buoy winds and one for the coincident ERS-1 algorithm derived winds. From Figure 21 it is clear that the AMI algorithm tends to bias its estimates towards low winds and does not report winds below 4 m/s. Since the AMI retrieval accuracy for low wind speeds was expected to be poor, algorithm retrievals below 4 m/s were not reported but were instead set to an invalid default wind speed of 51 m/s. The fact that the initial AMI wind algorithms underpredicted the true wind caused nearly 40% of the retrievals to appear to be less than 4 m/s when in fact only about 23% of the retrievals were made under conditions where the actual wind speed, according to buoys, was less than 4 m/s. The histogram in Figure 22 shows the RA wind speed algorithm to be performing somewhat better than the AMI algorithm. Figure 23 shows histograms of the coincident measurements of RA and buoy measured wave height and indicates a slight tendency for the wave height algorithm to favor a mean wave height of 2.5 m.

The scatterplots in Figures 24, 25 and 26 indicate algorithm performance as follows: AMI wind speed: bias +0.4 m/s, SD 4.1 m/s; RA wind speed: bias −0.2 m/s, SD 3.0 m/s; RA significant wave height: bias −0.1 m, SD 0.6 m.

AMI wind direction is measured with respect to true north and is defined as the direction from–which the wind is blowing. Scatterplots of AMI vs buoy wind direction indicate that almost 50% of the AMI retrievals are in error by approximately 180°. The 180° ambiguity problem can be removed by using a folded scale for the scatterplot which is accomplished by subtracting 180° from both buoy and AMI wind direction when these quantities exceed 180°. Such a plot is shown in Figure 27 and in this context the AMI wind direction is found to have a bias of −1.4° and a SD of 28°.

2.4 Future Work

As more data becomes available, investigations will be undertaken to determine retrieval algorithm dependence upon such parameters as buoy type (standard or continuous–average), AMI beam incidence angle, and air/sea temperature differences. One method of studying these dependencies is to use residual plots. An example of this technique is given in Figure 28, which in general shows the AMI wind speed algorithm retrievals to be biased low at small incidence angles and to be biased high at larger incidence angles. Further evaluation of the *Pierson [1983]* technique for averaging buoy measurements to reduce the comparison error is also planned.

Studies of buoy climatology for the NOAA network reveal an extremely low probability of occurance for winds above 15 m/s. Therefore, aircraft underflights are planned during the 1992 hurricane season for the purpose of collecting sufficient data in the 15 m/s to 24 m/s range to complete the performance assessment of AMI wind speed algorithm.

2.5 Conclusions

Based on comparisons with ocean buoys during the period November 1, 1991 through February 28, 1992, the ESA operational algorithm(s) retrievals of AMI wind speed and RA wind speed are relatively unbiased with standard deviations of 4.1 m/s and 3.0 m/s
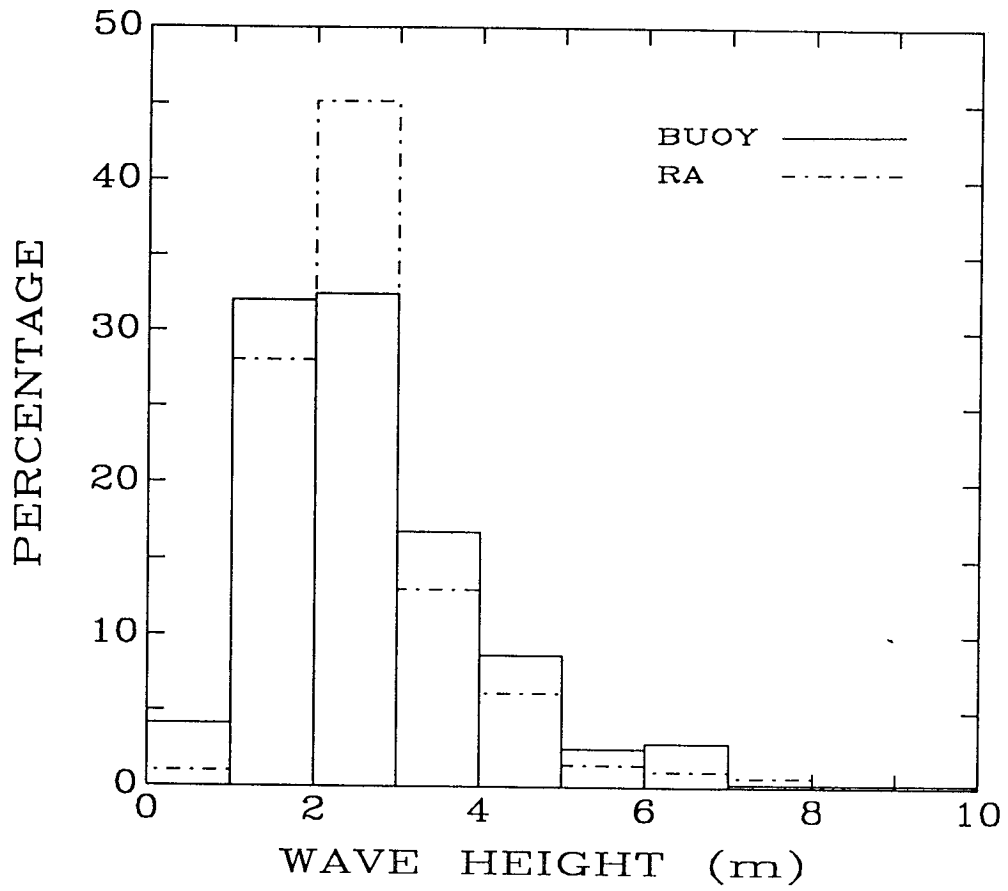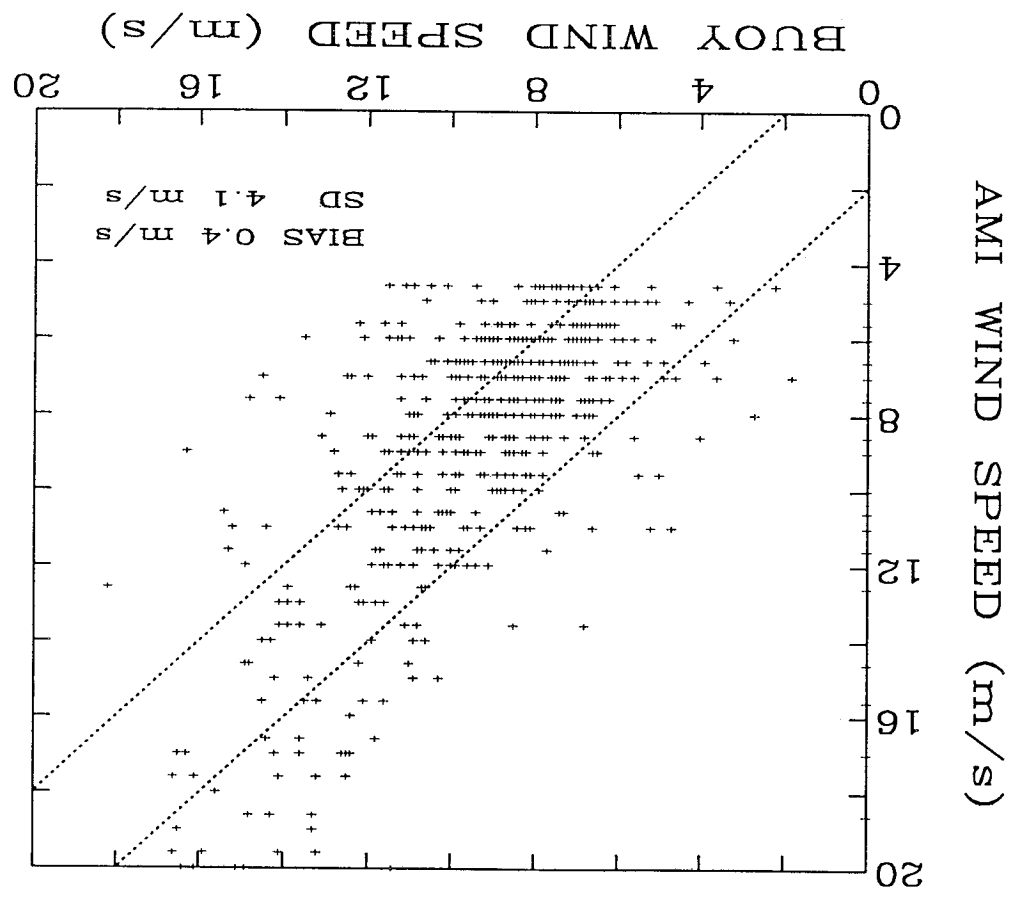
Figure 23. Distribution of buoy (solid line) and coincident RA (dot-dash line) retrieved wave height.

Figure 24. Scatterplot of the 577 coincident measurements of wind speed by the AMI and ocean buoys. The straight dotted lines indicate the ±2 m/s error bounds.

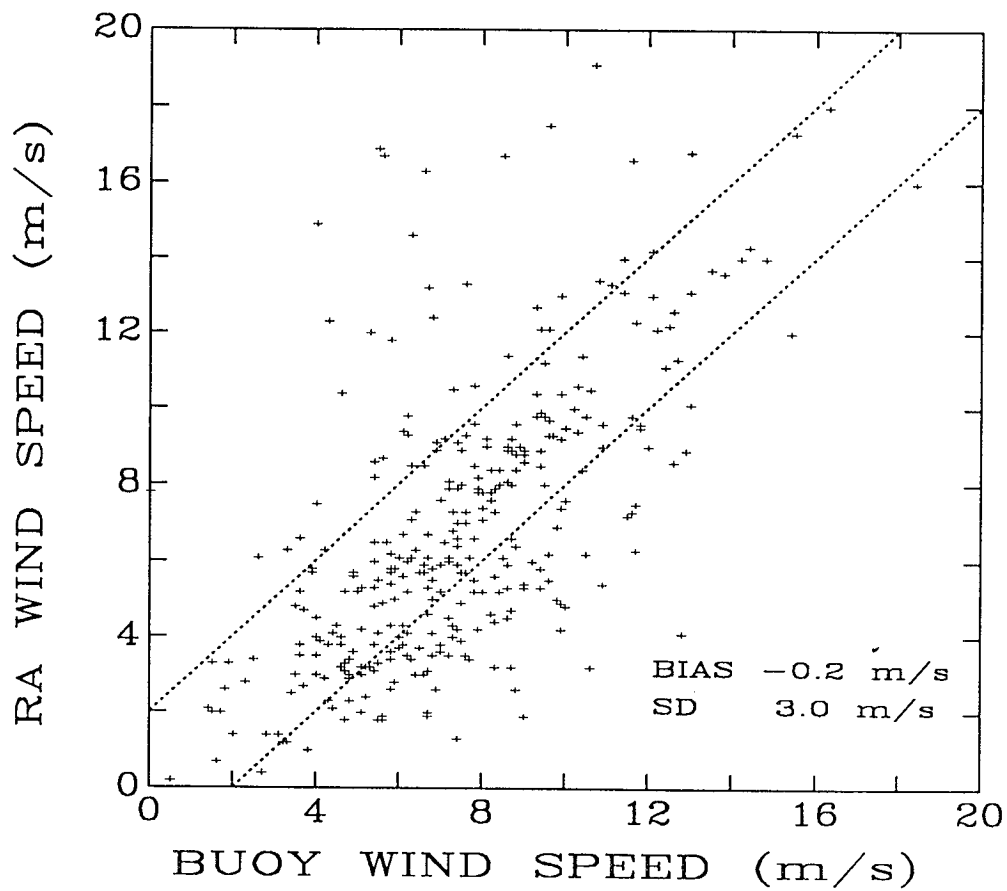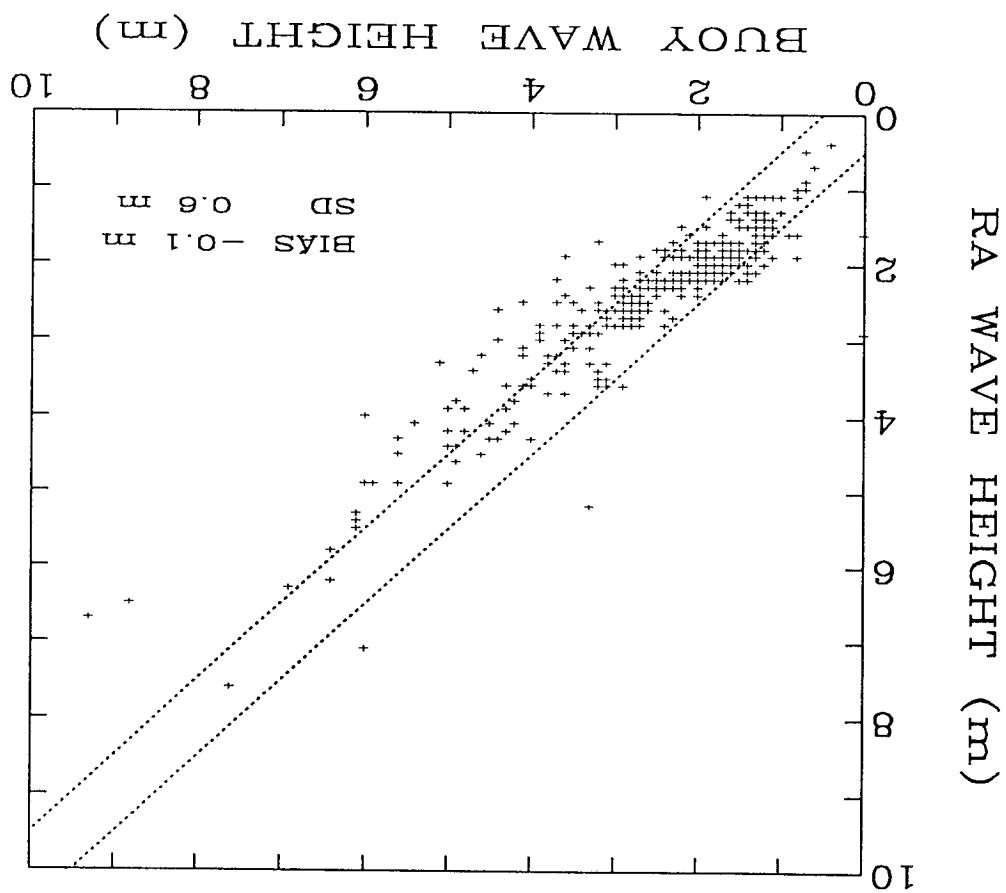Figure 25. Scatterplot of the 485 coincident measurements of wind speed by the RA and ocean buoys. The straight dotted lines indicate the ±2 m/s error bounds.

Figure 26. Scatterplot of the 485 coincident measurements of wave height by the AMI and ocean buoys. The straight dotted lines indicate the ± 0.5 m error bounds.
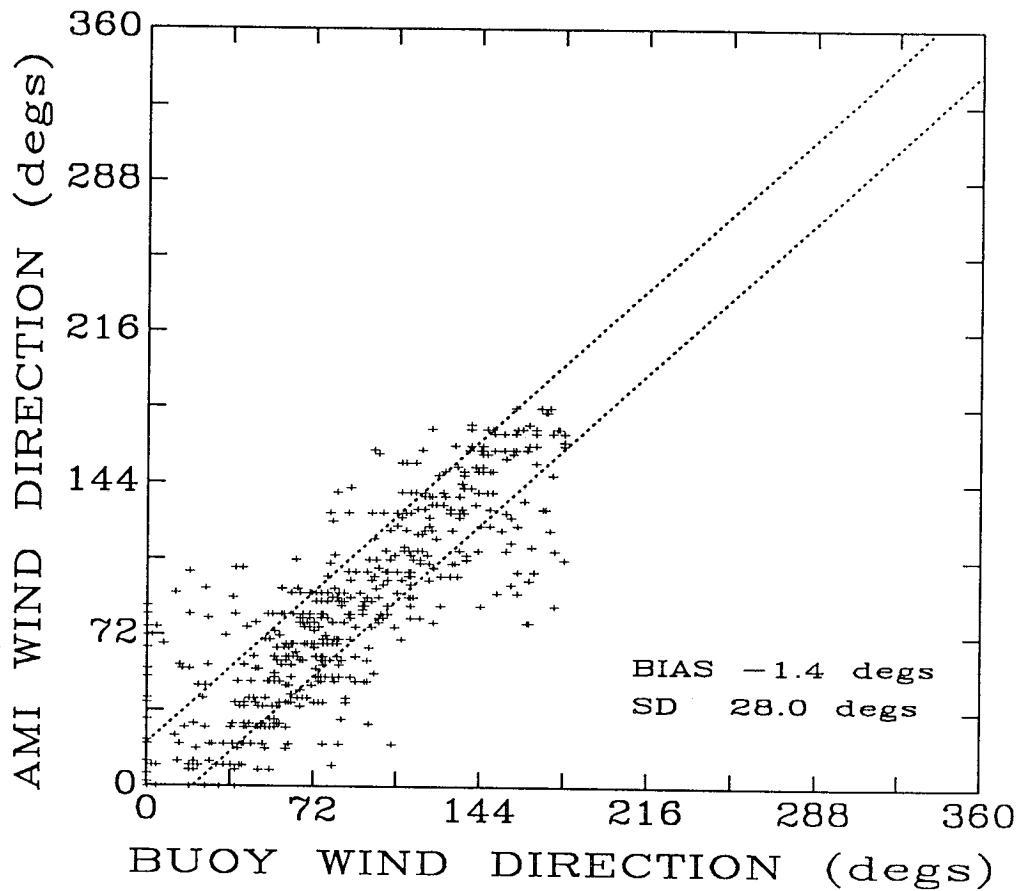
Figure 27. Scatterplot of the 577 coincident measurements of wind direction by the AMI and ocean buoys. The plotting scales have been folded to remove some 180° ambiguities in the AMI retrievals. The straight dotted lines indicate the ±20° error bounds.
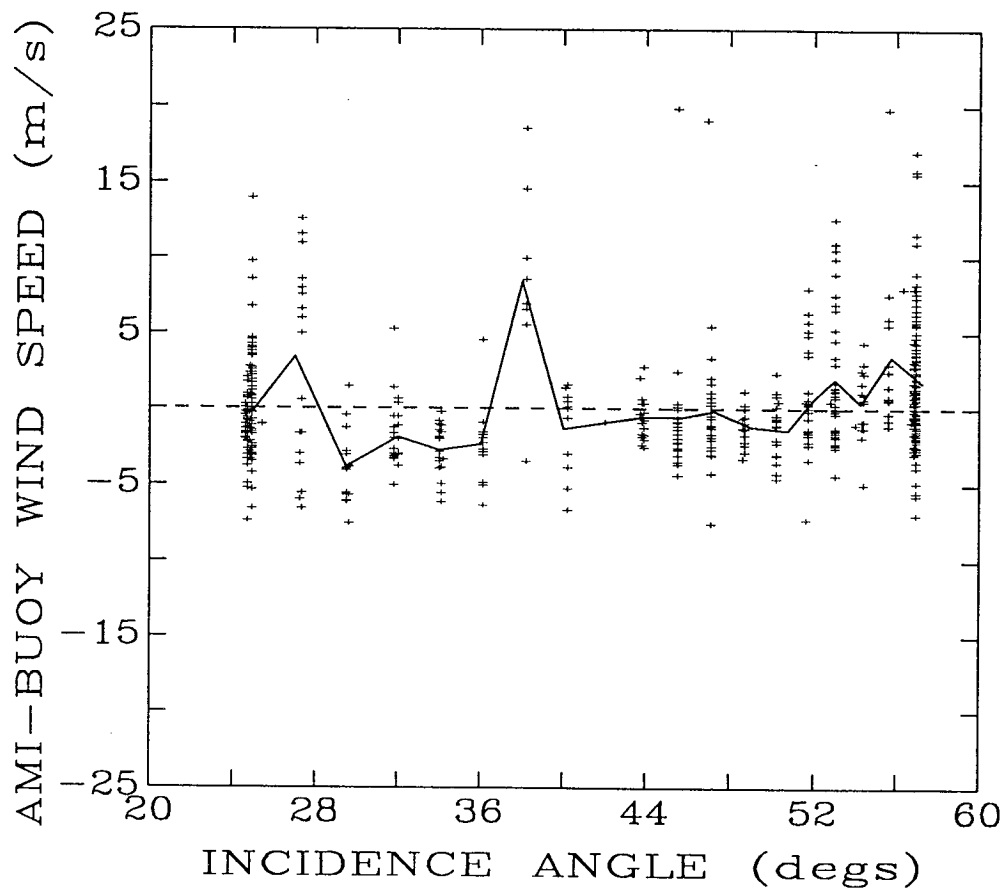
Figure 28. The difference between AMI and buoy measurements of
wind speed plotted as a function of AMI fore-beam incidence angle.
Note that the points in the plot fall into 19 vertical bins which
correspond with the 19 beam positions in the AMI swath. The solid
line is drawn through positions which are the average value of the
points in each of the 19 bins.

respectively. After removing 180° ambiguity errors, AMI wind direction retrievals were found to be unbiased with a standard deviation of ±28°. RA significant wave height retrievals are similarly unbiased with a standard deviation of 0.6 m. Because each of the ERS–1 wind speed and wave height algorithms underwent numerous changes during the validation period, the accuracy estimates presented here reflect the combined performance of several versions of each algorithm. Therefore, these performance figures can only be considered as interim assessments. As final versions of each algorithm are implemented, additional evaluation will be conducted to complete the validation.

REFERENCES

Gilhousen, D.B., E.A. Meindl, M.J. Changery, P.L. Franks, M.G. Burgin, and D. A. McKittrick, "Climatic Summaries for NDBC Data Buoys and Stations", National Data Buoy Center publication, NSTL, Ms., 1990.

Ezraty, R., "Etude de L'Algorithme D'Estimation de la Vitesse de Frottement a la Surface de la Mer" IFREMER, no. 85.2.42.5000. ESA contract 6155/85/NL/BI, June 1985.

Pierson, W.J., The Measurement of the Synoptic Scale Wind Over the Ocean, J. Geophys. Res., 88, 1683–1708, 1983.